Die approbierte Originalversion dieser Diplom-/Masterarbeit ist in der Hauptbibliothek der Technischen Universität Wien aufgestellt und zugänglich.
http://www.ub.tuwien.ac.at

The approved original version of this diploma or master thesis is available at the main library of the Vienna University of Technology.
http://www.ub.tuwien.ac.at/eng

Unterschrift des Betreuers

TECHNISCHE UNIVERSITÄT WIEN

DIPLOMARBEIT

Dependence of Tokamak Confinement on ELM Power Loss

ausgeführt am Institut für Angewandte Physik der
Technischen Universität Wien und
am Max-Planck-Institut für Plasmaphysik

unter der Anleitung von

Univ.-Prof. Mag.rer.nat. Dipl.-Ing. Dr.techn.
Friedrich Aumayr

und

Univ.Doz. Dipl.-Ing. Dr.techn. Elisabeth Wolfrum

durch

Marko W. Mayr
Leebgasse 79/6, 1100 Wien

12. Dezember 2016

Unterschrift Student

Abstract

The energy confinement time τ_E is a measure of how long energy remains in a plasma. Multi-machine studies of τ_E have been used to derive a scaling law for tokamak confinement based on engineering parameters. Comparing the measured confinement time to the predicted confinement time results in the H-factor, which is equal to one if the scaling is perfect. An H-factor of less than one describes a scenario where the plasma does not perform as well as predicted.

The occurence of Edge Localised Modes (ELMs) in the high confinement mode of a tokamak limits the height of the edge transport barrier, known as the pedestal. A crash due to an ELM is associated with particle and energy transport outwards of the confined region and occurs when a critical pedestal pressure gradient is reached.

According to measurements and scalings, increasing the input power has a negative effect on τ_E. But the effect of the power lost due to ELMs on the confinement time has so far not been taken into account for scalings of the energy confinement time. In this thesis, the energy confinement time scaling is recharacterised by including the power losses due to ELMs and it is shown, using data from ASDEX Upgrade, that no improvement can be seen by doing so. A higher deviation in the H-Factor for $P_{reduced} = P_{heat} - P_{ELM}$ compared with the H-factor of the P_{heat} scaling attest to this finding. In order to be able to interpret the scalings, parameter correlations, e.g. for the heating power and the ELM loss power, have been computed. It was also tried to find scaling laws for ELM losses, which were split into scalings for the ELM frequency and for the energy loss due to ELMs. These scalings however were more difficult to interpret and were found to be more inaccurate resulting in a high root-mean-square error. Indications will be presented which show a positive trend between ELM losses and the pedestal pressure.

Zusammenfassung

Die Energie-Einschlusszeit τ_E ist eine Messgröße, die beschreibt, wie lange Energie in einem Plasma eingeschlossen bleibt. Studien für die Tokamak-Einschlusszeit mit mehreren Tokamaks wurden verwendet um Skalierungen abzuleiten, die auf sogenannten Engineering-Parametern beruhen. Der Vergleich zwischen gemessener und errechneter Einschlusszeit resultiert in dem sogenannten H-Faktor, welcher den Wert eins annimmt, wenn die Skalierung perfekt ist. Ein H-Faktor, der niedriger als eins ist beschreibt ein Szenario, in welchem das Plasma für den Teilcheneinschluss schlechtere Eigenschaften aufweist als berechnet.

Das Auftreten von sogenannten Edge Localised Modes (ELMs), also von lokalisierten Moden im Plasmarand, in der High Confinement Mode eines Tokamaks beschränkt die Größe der Randtransportbarriere, welche auch Pedestal (Podest) genannt wird. Ein Zusammenbruch wegen einer ELM ist mit Teilchen- und Energietransport aus dem Plasma hinaus assoziiert und passiert, wenn ein kritischer Pedestaldruckgradient erreicht wird.

Den Messungen und Skalierungen zufolge hat die Erhöhung der Heizleistung einen negativen Effekt auf τ_E. Jedoch wurde bislang noch nicht evaluiert, in welcher Form die durch ELMs verlorene Leistung Skalierungen der Einschlusszeit beeinflusst. In dieser Masterarbeit wurde die Skalierung der Energie-Einschlusszeit durch das Einbeziehen ebendieser Leistung recharakterisiert. Es wird mithilfe von ASDEX-Upgrade Messungen gezeigt, dass keine Verbesserung der Skalierung erreicht wird. Eine höhere Standardabweichung im H-Faktor für $P_{reduced} = P_{heat} - P_{ELM}$ verglichen mit dem H-Faktor für die P_{heat}-Skalierung unterstützen diese Beobachtung. Um die Skalierungen interpretieren zu können, wurden Parameterkorrelationen - zum Beispiel für P_{heat} oder die Verlustleistung durch ELMs - berechnet. Des Weiteren wurde versucht Skalierungen für die ELM-Verluste, welche in die Anteile der ELM-Frequenz und des Energieverlusts aufgeteilt wur-

den, zu finden. Jedoch war die Interpretation dieser Skalierungen problematisch, da sie, wie durch einen hohen RMS-Fehlerwert beschrieben wird, unpräzise zu sein scheinen. Hinweise für einen positiven Trend zwischen den ELM-Verlusten und dem Pedestaldruck werden jedoch gezeigt.

Contents

1 Introduction **1**

2 Tokamak **9**

2.1 Overview 9

2.2 ASDEX Upgrade 11

2.2.1 Heating mechanisms 11

3 Theory **13**

3.1 H-mode 13

3.2 Edge Localised Modes 14

3.2.1 Particle and Energy Losses due to ELMs 18

3.2.2 Extrapolation to ITER 20

3.3 Scaling Laws 21

3.4 High Field Side High Density Front 23

4 Analysis Method **25**

4.1 Diagnostics 25

4.1.1 Electron Cyclotron Emission (ECE) Radiometry 25

4.1.2 Thomson Scattering 28

4.1.3 Lithium-Beam Diagnostic 28

4.1.4 Interferometry 28

4.2 Equilibrium Reconstruction 28

4.3 AUG Pedestal Fitting 29

4.3.1 ELM Synchronisation 30

4.3.2 Fit Functions/Fitting Procedure 31

4.3.3 Shifting the Data 32

4.3.4 Pedestal Top Values 33
4.4 Database 34
4.4.1 Used Data 34
4.4.2 Used Parameters 36
4.4.3 Computing W_{MHD}^{pe} 39
4.4.4 Data Regression 40
4.4.5 Parameter Correlations 41

5 Results **43**
5.1 Parameter Correlations 43
5.2 Scaling Laws for τ_E 44
5.3 H-Factor 47
5.4 Ordering Parameter for ELM losses 49
5.4.1 Scaling for ELM Energy Losses ΔW_{MHD} 50
5.4.2 Scaling for ELM Frequency f_{ELM} 51

6 Conclusion and Outlook **55**

Chapter 1

Introduction

The supply of energy faces difficulties due to increasing population growth as well as increasing per capita energy consumption. To overcome these challenges the international community longs for efficient, clean and, ideally, cheap energy production. In particular, European countries are currently trying to reduce the consumption of fossil fuels, which still have a large share in the overall energy production.

A candidate for a solution of this problem is nuclear fusion, which is a process of nuclear rearrangement in which two light atoms merge to a heavier atom and other reaction products which carry away excess energy in the form of kinetic energy. This energy is of the order of the binding energy between the nuclei.

Like other stars, the sun produces energy using nuclear fusion. The process reads:

$$p + p \rightarrow \ D + e^{+} + \nu_e \tag{1.1}$$

$$D + p \rightarrow \ {}^{3}_{2}He + \gamma \tag{1.2}$$

$${}^{3}_{2}He + \ {}^{3}_{2}He \rightarrow \ {}^{4}_{2}He + 2p \tag{1.3}$$

which corresponds to a resulting process of:

$$4p \rightarrow \ {}^{4}_{2}He + 2e^{+} + 2\nu_e + 26.7\,\mathrm{MeV}. \tag{1.4}$$

In the above equations, the following abbreviations were used:

- p ... Proton
- e^+ ... Positron
- D ... Deuterium nucleus
- ν_e ... Electron neutrino
- γ ... Photon
- ${}^4_2He$ ... Helium nucleus

Different reactions have different cross sections which is a measurement of how likely a fusion process is with varying impact energy (kinetic energy of participants). The cross sections for fusion (see figure 1.1) suggest the use of Deuterium and Tritium. This is because of the peak in the cross section for relatively low energies. The corresponding reaction is

$$D + T \rightarrow {}^4_2 He + n + 17.59\,\mathrm{MeV}, \tag{1.5}$$

where α represents a Helium nucleus and n represents a neutron. The excess energy of 17.59 MeV results from a mass deficit of 0.01875 m_p with m_p being the mass of a proton.
A low impact energy of the reaction participants leads to a small cross section because the energy is insufficient to overcome the Coulomb barrier of the electromagnetic interaction. Only the effect of quantum mechanical tunneling makes it possible to fuse atoms at lower impact energies.

The advantages of nuclear fusion are cheap and practically limitless fuel as well as low radioactivity levels compared to nuclear fission. Research on the efficient use of nuclear fusion for civilian purposes has been carried out since the 1950s but a fusion reactor which produces more energy than it consumes has not yet been built. Over the course of decades fusion devices have become more sophisticated and an internationally funded project currently under construction in France is designed to facilitate ignition, which means that the energy produced in the fusion process is enough to compensate the cooling due to energy losses and to sustain the fusion process without external heating. This project was named

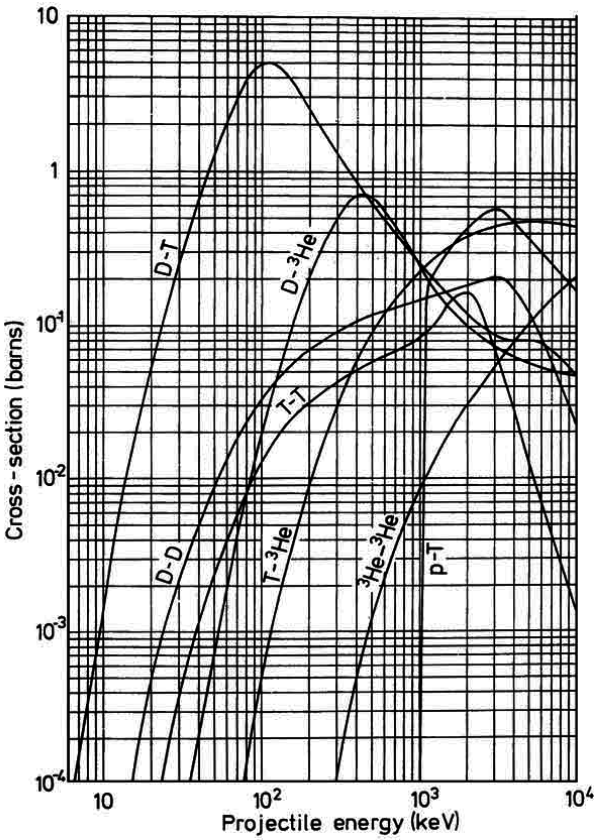

Figure 1.1: Cross-sections of the most commonly discussed fusion reactions plotted against the impact energy on a logarithmic scale. Taken from [9].

ITER, which is an English acronym for "international thermonuclear experimental reactor" and the Latin word for "the way". ITER will be the next step on the way to an operating nuclear fusion power plant with an anticipated power production of 500 MW for 400 seconds [28].

The power balance in a tokamak plasma is

$$P_{heat} + P_{\alpha} = P_{loss} \ , \tag{1.6}$$

where P_{heat} is the external heating power and P_{α} is the heating power due to alpha particles which are produced in the fusion process (see equation 1.5) and are confined by a magnetic field thus being able to further heat the plasma. P_{loss} is the rate of energy lost from the plasma per time.

For ignition to be possible, certain conditions for the particle density n, the temperature T and the energy confinement time τ_E, which is defined as

$$\tau_E = \frac{W}{P_{heat} - dW/dt} \ , \tag{1.7}$$

have to be met. In this equation, W is the stored plasma energy. The Lawson criterion for ignition states that the triple product of n, T and τ_E has to overcome a value of 3 to $5 \times 10^{21} m^{-3} keV s$, depending on the profiles of n and T [30]. Thus, one could naively assume that it would be best just to increase the three parameters to their highest possible values. But raising all parameters turns out to be a difficult task since the parameters are related to each other. As can be seen in figure 1.2, the product of the density and the energy confinement time has a global minimum at a temperature of about 30 keV. After fixing this temperature the triple product can be reached by raising n or τ_E. For magnetic confinement fusion devices it is difficult to raise the density to high levels without this leading to plasma disruption and therefore the confinement time has to be as high as possible whereas in inertial confinement fusion the density is increased as much as possible, but only for short times.

Since the energy confinement time is also dependent on T, using the minimal temperature value turns out not to be the optimum condition. The operational

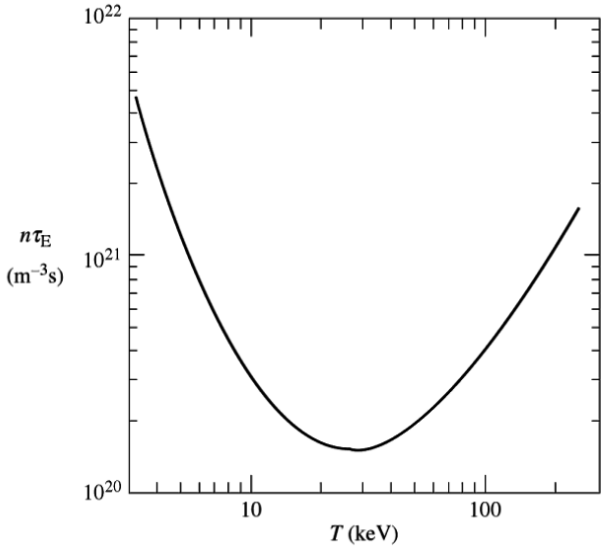

Figure 1.2: The value of the product of n and τ_E required to obtain ignition as a function of T. Taken from [30].

window for ITER is planned to be between 10 and 15 keV.

Confining a fusion plasma is a difficult task and several methods to do this have been proposed. One method is the magnetic confinement, which uses strong magnetic fields preventing the majority of the plasma particles from escaping. The reason for this is the Lorentz force

$$m \cdot \frac{d\boldsymbol{v}}{dt} = q(\boldsymbol{v} \times \boldsymbol{B}) \ , \tag{1.8}$$

which acts upon charged particles and leads to a gyration around the magnetic field lines with the frequency

$$\boldsymbol{\omega_c} = \frac{q \cdot \boldsymbol{B}}{m} \ , \tag{1.9}$$

where $\boldsymbol{v}$ is the velocity of the particle, q is the electric charge of the particle, $\boldsymbol{B}$ is the magnetic field strength and m is the mass of the particle.

The so-far most successful devices use toroidally bent and closed magnetic field lines. Unfortunately, this simple arrangement of the magnetic field coils comes along with some inconveniences, like drift phenomena that prevent good confinement. Reasons for this are for example the decreasing magnetic field with increasing radius or a pressure gradient. In the first case, the Lorentz force

changes its magnitude over the tokamak radius and therefore is not constant over the gyration orbit of the charged particles. This will lead to an orbit which has a greater radius at the low field side and vice versa. In the second example one finds that a "diamagnetic" current will evolve in the vicinity of a pressure gradient which will result in a magnetic field which mitigates the original magnetic field. In the latter example no mass is being transported.

These drifts can be cancelled out using helically twisted field lines which are a result of using a combination of a toroidal and a poloidal field. One device which uses this phenomenon is a tokamak, which will be described in detail in chapter 2.

It has been shown that the confinement time for tokamaks (which until now can only be operated in pulses) has a strong positive correlation with the machine size. This explains that new experiments like ITER are designed to have larger dimensions which are necessary for reaching the conditions needed to gain energy from the fusion process. Unfortunately, we do not know whether the physics used for simulations describing the impact of the high temperatures, high particle densities and large dimensions on the plasma behaviour for ITER is complete and therefore it is not possible to make an accurate prediction using simulations. Results from measurements carried out on present-day machines like JET in the United Kingdom or ASDEX Upgrade in Germany can be extrapolated to predict the effects of changing certain parameters, namely the pedestal top temperature and the confinement time, in the operation onto a bigger machine. For this purpose scaling laws have been evolved which try to describe these quantities using either dimensionless "physics" parameters or engineering parameters. Physics parameters describe the plasma properties whereas engineering parameters are determined by operational constraints and describe the machine properties.

ITER will operate in the so-called high confinement mode (or H-mode) regime which will be described in section 3.1. In this regime instabilities occur that periodically expel particles and therefore reduce the energy stored in the plasma. Those instabilities are called Edge Localised Modes or ELMs, occur on millisecond time scales and have a repetition frequency from a few Hz up to several hundred Hz. They will be discussed in section 3.2.

In this thesis the power lost due to these modes will be included into the scalings for the confinement time and it will be shown whether it brings an improvement to the scaling or not. Furthermore co-dependencies of the parameters included in the confinement time scaling will be determined. Using data from ASDEX Upgrade, the H-factor, which is the confinement normalised to the prediction, will be determined considering also the losses due to Edge Localised Modes.

Chapter 2

Tokamak

2.1 Overview

The word "tokamak" is a Russian acronyme for "toroidal chamber in magnetic coils". As has been stated in the introduction, the Tokamak is a promising concept for magnetic confinement fusion. It was developed in the Soviet Union thanks to theoretical ideas of Igor Yevgenyevich Tamm and Andrei Dmitrievich Sakharov. The initial principles of confinement in a toroidal chamber using magnetic coils were first formulated in October 1952 [26]. Figure 2.1 shows the concept of a tokamak.

In a tokamak the toroidal field is created by the toroidally assembled magnetic field coils and the poloidal field is created by a toroidal plasma current I_p. I_p is induced by increasing the current through a solenoid located in the cavity in the center of the torus. Now the plasma acts as the secondary winding of a transformer. The disadvantage of using a transformer is a temporally limited operation since the current through the solenoid cannot be increased infinitely. Steady-state operation is not limited to a short pulse since it does not need a transformer to generate a current in the plasma but relies on a current which is non-inductively driven. This feature makes it very attractive for the use in a power plant and is therefore a topic of ongoing research [19] [20].

The position of the plasma volume and its shaping can be controlled using

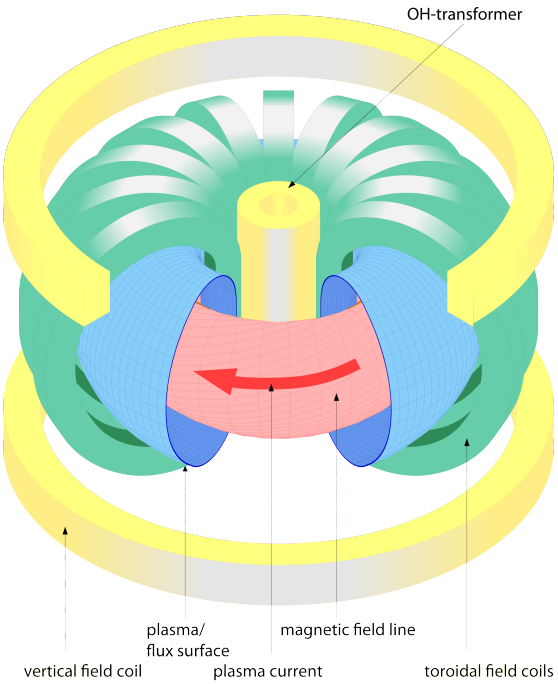

Figure 2.1: Schematic view of a tokamak machine. Figure reproduced from AUG database.

poloidal field coils which generate a vertical magnetic field. The shaping of a tokamak plasma is mostly described by the triangularity δ, the elongation κ, the geometrical minor radius a_m and the geometrical center of the plasma R_{geo}, which will be described in detail in section 4.4.2.

The helically twisted magnetic field lines form layers of constant flux. On these layers, which are called magnetic surfaces, the pressure is constant and therefore the pressure gradient is perpendicular to the surface. If one follows one of these magnetic field lines, one is able to find the safety factor q, which is defined as the gradient of the toroidal flux with poloidal flux or, more simply, as the number of toroidal orbits of the magnetic field lines per poloidal orbit.

There are two common types of plasma oparation which are distinguished by the use of a divertor in one case and that of a limiter in the other case. A limiter is a device which intercepts the flux surfaces thereby creating the last closed flux surface. The divertor is located underneath the so-called X-point, which is a point in the poloidal projection in which B_p, which is the poloidal magnetic field, has a null. In a device using a divertor, the last closed flux surface, or "separatrix",

is only influenced by the magnetic field. The region of plasma which is located outside of the last closed magnetic flux surface is called scrape-off layer (SOL).

This thesis uses experimental data from the tokamak "ASDEX Upgrade" in Garching, Germany.

2.2 ASDEX Upgrade

ASDEX[1] Upgrade (AUG) is a tokamak equipped with a tungsten divertor, which protects the walls of the reactor vessel from erosion. This is important to ensure the durability of the plasma facing components (PFCs). Tungsten is the material of choice because of its low erosion rate and its low tritium retention ([15] [16]), the latter being relevant for research for a fusion reactor. Interactions with the tungsten surface take place outside of the confined plasma.

The following table gives an overview of ASDEX Upgrade's engineering parameters.

Plasma current (I_p)	0.4-1.6 MA
Maximum magnetic field (B_T)	3.1 T
Heating power (P_{heat})	up to 30 MW
Major plasma radius (R_0)	1.65 m
Minor horizontal plasma radius (a)	0.5 m
Minor vertical plasma radius (b)	0.8 m
Triangularity (δ)	up to 0.4
Plasma volume (V)	14 m^3

Table 2.1: Engineering parameters of ASDEX Upgrade.

2.2.1 Heating mechanisms

The simplest form of heating the plasma is Ohmic heating. On a microscopic scale, Ohmic heating takes place because of Coulomb interactions between electrons and ions. Scattering of charged particles leads to thermal motion. Due

[1] Acronym for axial symmetric divertor experiment.

to the fact that the dissipation of the plasma current depends on the plasma temperature (decreasing resistance with increasing temperature), temperatures higher than a few keV are impossible to reach [8]. The amount of heat produced is described in Joule's first law:

$$H \propto I^2 \cdot R \cdot t \ , \tag{2.1}$$

where H is the heat produced, I is the flowing current, R is the resistance and t denotes the time.

Heating the plasma in addition to Ohmic heating is crucial to reach the energies required to start the fusion reaction. At ASDEX Upgrade the heating power P_{heat} is mainly applied via radio waves and microwaves as well as through injection of high energy particles. The total additional heating power is about 30 MW of which

- the electron cyclotron resonance heating (ECRH), which uses microwaves, contributes with 4 MW,
- the ion cyclotron resonance heating (ICRH), which uses radio waves, contributes with 6 MW and the
- neutral beam injection contributes with 20 MW.

With these heating methods (but mainly via high energy particles) an ion temperature of more than 10^8 K can be realised [5].

Chapter 3

Theory

This chapter will give an overview over the most relevant theoretical aspects in tokamak-related plasma edge physics which are essential for this work.

3.1 H-mode

Plasma parameters like the electron density and the electron temperature are constant on a flux surface but vary strongly along the radius in the plasma edge region. If their values are plotted against the tokamak radius in a poloidal cross section, characteristic profiles can be identified. For reasons of convenience, the normalised poloidal radius of the tokamak ρ_{pol} can be introduced:

$$\rho_{pol} = \sqrt{\frac{\psi_{axis} - \psi}{\psi_{axis} - \psi_{seperatrix}}}, \tag{3.1}$$

ψ being the poloidal magnetic flux, ψ_{axis} being the flux at the magnetic axis which is also the plasma center and $\psi_{separatrix}$ being the flux at the separatrix. On the ρ_{pol}-abscissa, 1 indicates the radial position of the separatrix.

The main operational regimes of a tokamak are primarily controlled by the power injected into the plasma P_{heat}. If a certain power threshold is reached, the L-mode or low confinement mode will undergo a transition to the H-mode or high confinement mode, which shows distinct properties like an almost twice as large value of the energy confinement time [28]. The H-mode was discovered at ASDEX in 1982 [29]. The reason for this transition in confinement properties is not yet fully understood but it is agreed upon that if a certain heating power threshold

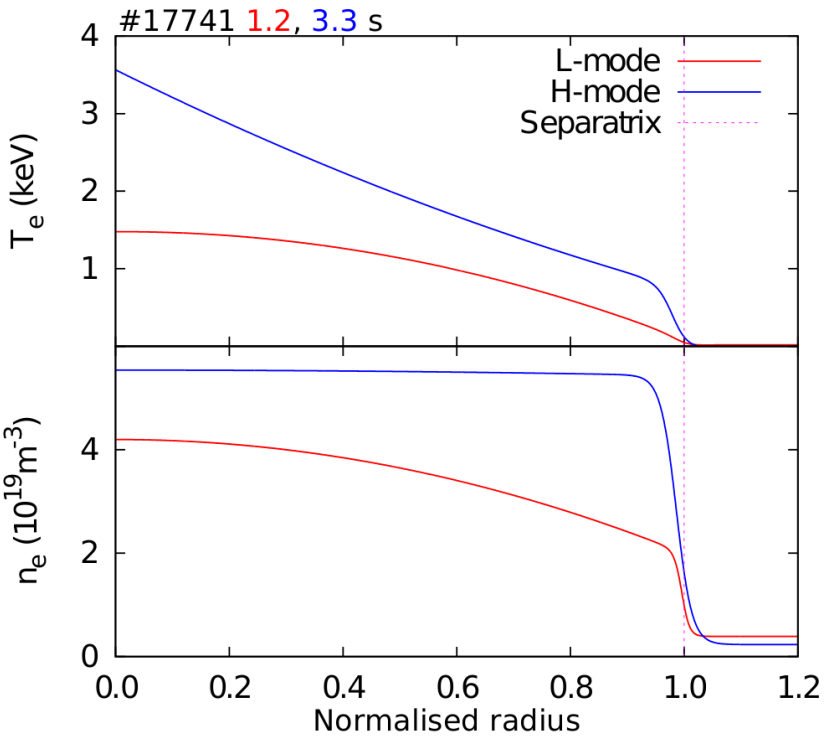

Figure 3.1: Electron temperature and electron density in H-mode (blue) and in L-mode (red) plotted against the normalised radius for the AUG discharge #17741. Taken from [2].

is reached, an edge transport barrier evolves which hinders radial transport and therefore also particle and energy losses. This transport barrier is defined by an increased pressure gradient compared to L-mode in the outermost $\sim 2\,\mathrm{cm}$ of the region of closed magnetic surface lines (inside of the separatrix). Increased gradients in the electron temperature T_e and density n_e lead to significantly increased total values of these parameters across the whole plasma. The slim region described above is called the edge pedestal, because the profiles of the core plasma lie on top of it. Figure 3.1 shows the raised T_e and n_e levels in H-mode compared to L-mode. It is believed that the L-H transition is a result of suppressed turbulence due to the evolution of a radial electric field and corresponding $E \times B$ shearing [27] [2].

3.2 Edge Localised Modes

Edge Localised Modes (ELMs) are plasma instabilities linked to the high pressure gradient in H-mode. They periodically expel particles and energy of the order

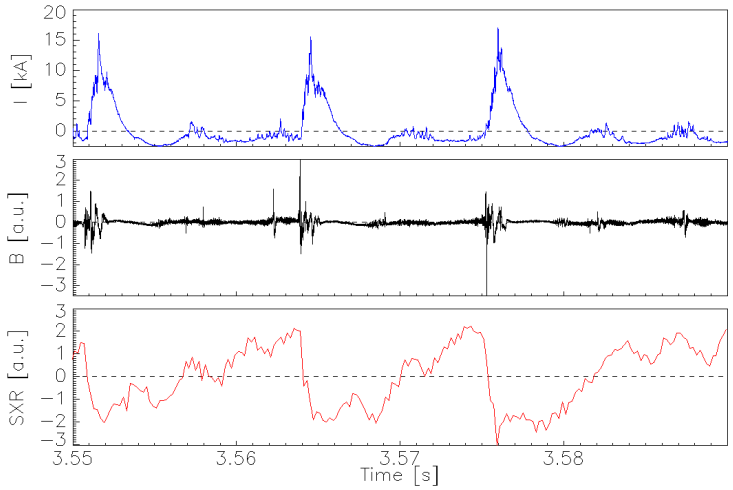

Figure 3.2: Signature of an ELM in the signals of the inner scrape-off layer divertor current $I_{polsoli}$, the magnetic pick-up coils and the soft X-ray radiation in a time interval of 0.04 s. Shot #23418 was used for this plot.

of a few percent up to 30 % of the stored energy from the magnetically confined plasma volume which are then guided to the divertor or other PFCs via open magnetic field lines. During an ELM the pressure gradient drops significantly due to the drop of the density and the temperature gradients as can be seen in figures 3.3 and 3.4. The energy lost due to the reduction of the plasma pressure is

$$\Delta W^{pe}_{MHD} = \frac{3}{2} \int \Delta p dV, \tag{3.2}$$

causing high heat loads on the PFCs that can even melt because of ELMs.

The ELM duration as well as the recovery time after an ELM crash is very variable. An ELM can last for a few milliseconds and may occur with a frequency between a few Hertz and up to more than 1000 Hertz [22], depending on the ELM type. The traditional method of measuring ELMs is detecting H_α radiation, which is not reliable in a tokamak equipped with tungsten coated divertor tiles. Alternatively, ELMs can for example be detected via the observation of the poloidal divertor current, the magnetic equilibrium measured by pick-up coils or soft x-ray radiation (see figure 3.2).

ELMs are usually classified into three different types:

- **Type-I ELMs**
- **Type-II ELMs**

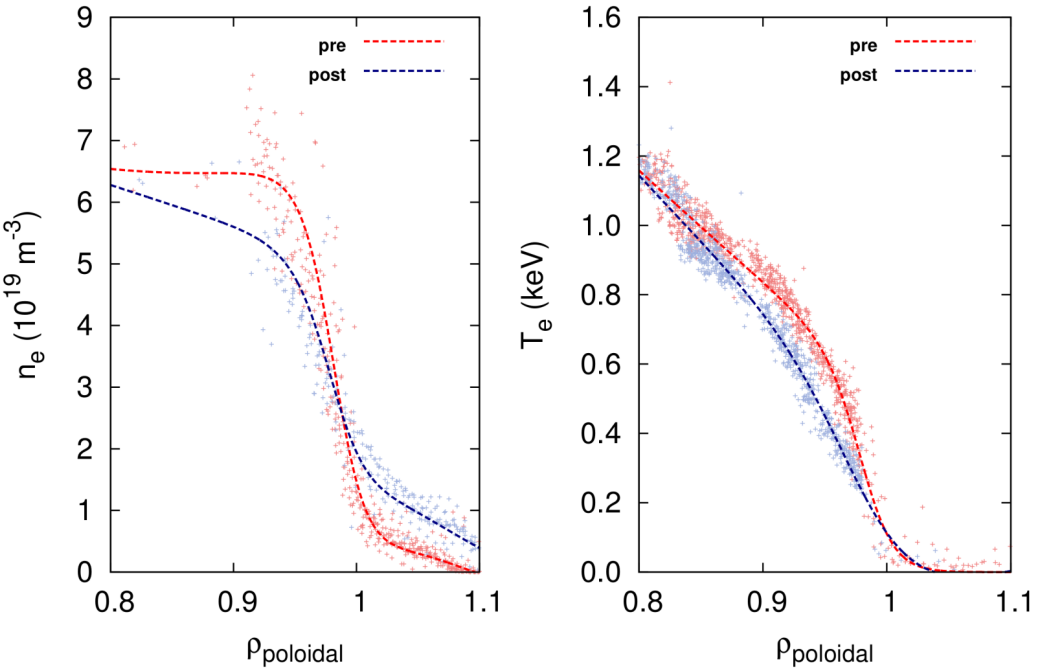

Figure 3.3: Electron temperature and density profiles before (pre) and after (post) an ELM. The data used is taken from shot #34332. It can be seen that the pedestal values drastically decrease immediately after the crash takes place. $\rho_{poloidal}$ is the normalised radius and the value of 1 corredsponds to the separatrix at the outer midplane. The fits have been performed using a modified tanh-function.

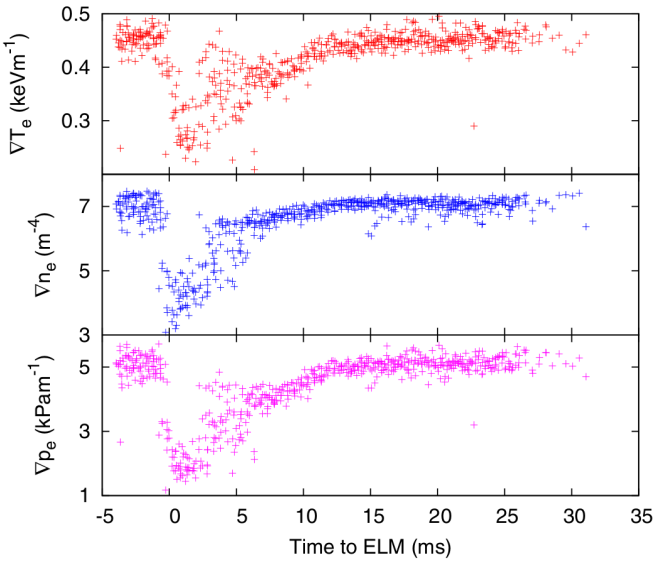

Figure 3.4: Electron temperature (red), electron density (blue) and electron pressure (pink) at the pedestal top relative to an ELM crash. Taken from [2]

- **Type-III ELMs**

In this thesis only Type-I ELMs were taken into account. They take place in operational regimes which have the best confinement times. They are characterised by the large loads of particles and energy which are lost due to these ELMs. The frequency of Type-I ELMs increases with increasing heating power. The instability occurs, when the critical limit α_{crit} of the normalised pressure gradient, which varies as a function of the pedestal width [2], is reached. Type-I ELMs usually define a reproducible regime [25]. Type-II and Type-III ELMs generally have a higher frequency than Type-I ELMs but a smaller energy loss. Thus plasma facing components will not be affected by the heat loads as strongly as in Type-I ELMs.

Although a complete theory of ELMs is still the subject of ongoing research, it is believed that ELMs can be described as peeling-ballooning modes, which are magnetohydrodynamic instabilities. The pressure gradient at the plasma edge causes an oppositely directed force to the magnetic field line tension. At the low field side the unfavourable addition of decreasing magnetic field strength and decreasing pressure with increasing radius are destabilising and lead to ballooning MHD modes. A current driven instability, the peeling mode was added to the theory because of the inability of the ballooning mode theory to describe why the pressure gradient stays constant a few milliseconds before the ELM crash occurs [25].

The pedestal density recovers at a different speed than the pedestal temperature, which can be seen in figure 3.4. As stated above, a phase of constant pressure gradient after the recovery can be observed and of which the temporal length cannot be predicted. This means that the last phase of ELMs seems to be determined by a yet unknown parameter.

Mitigation techniques for ELMs are areas of current research but in spite of the negative effects mentioned before, ELMs are very useful when it comes to decreasing the amount of impurities in the plasma which is important for a reduction of the energy lost due to impurity radiation [3].

Since the occurrance of an ELM places a limitation on the pedestal, and the pedestal is one of the factors which dominates global confinement, understanding

the ELM trigger is important to model future devices. The fact that high energy loads to the divertor could cause serious damage in tokamak operation using larger devices underlines the importance of understanding ELMs.

3.2.1 Particle and Energy Losses due to ELMs

To understand the mechanisms which cause Type I ELM energy losses, dependencies on plasma parameters have to be found. The normalised energy lost during an ELM event $\Delta W_{ELM}/\Delta W_{ped}$ decreases with increasing pedestal density [13]. The reason for this seems to be a reduction in the temperature drop rather than a reduction in the density drop. This implies that the mechanism which governs the energy loss also changes with increasing pedestal density. A parameter which fits the normalised ELM energy loss more accurately over a range of different experiments is the collisionality ν^*_{ped} of the pedestal plasma, which can be seen in the comparison of figures 3.5 and 3.6. [13] uses the following definition for the evaluation of ν^*_{ped}:

$$\nu^*_{ped} = \frac{R \cdot q_{95}}{\epsilon^{3/2} \cdot \lambda_{e,e}} \quad . \tag{3.3}$$

In the above equation, R is the major tokamak radius, q_{95} is the safety factor, which gives the number of poloidal orbits of a magnetic field line per toroidal orbit measured at 95% of the flux, ϵ is the inverse aspect ratio (a/R) with a being the minor radius. $\lambda_{e,e}$ is the electron-electron Coulomb collision mean free path and is defined in this calculation as

$$\lambda_{e,e} = 1.7 \cdot 10^{17} \frac{T^2_{e,ped}}{n_{e,ped} \cdot ln(\Lambda_e)} \quad . \tag{3.4}$$

For the calculations in this thesis the definition of Λ_e was obtained from [23] and reads

$$ln(\Lambda_e) = 31.3 - ln(\frac{\sqrt{n_e}}{T_e}) \quad . \tag{3.5}$$

Figure 3.6 was reconstructed with the data used in this thesis and the result is shown in figure 3.7. It shows that due to the high scatter and the small range available it is not useful to choose the collisionality as a parameter to describe ELM losses in this thesis.

The collisionality is a measure of how many collisions an electron undergoes

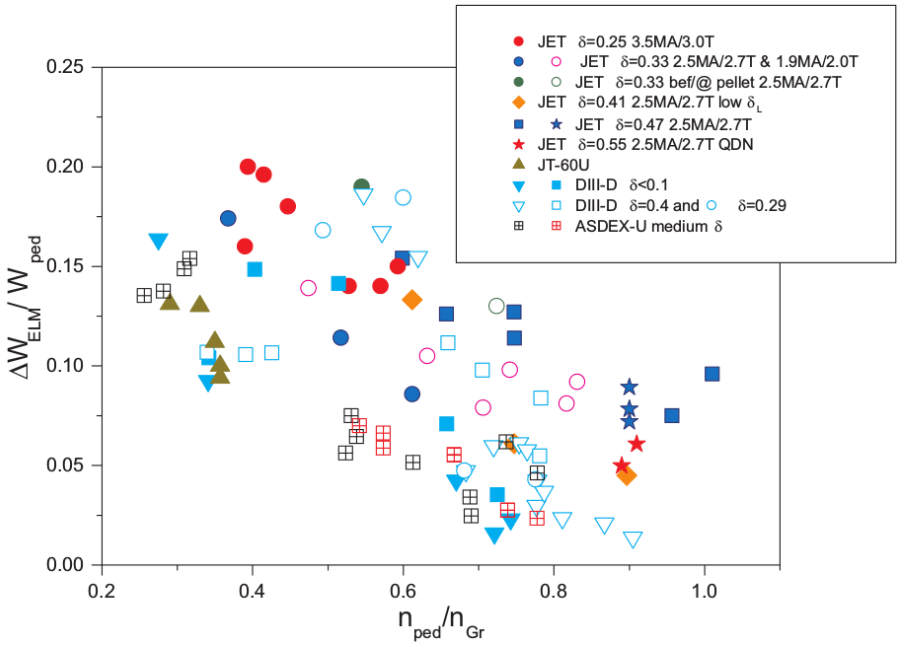

Figure 3.5: The normalised ELM energy loss is plotted against the pedestal density normalised to the Greenwald density limit for data points gathered from AUG, DIII-D, JT-60U and JET. Taken from [13].

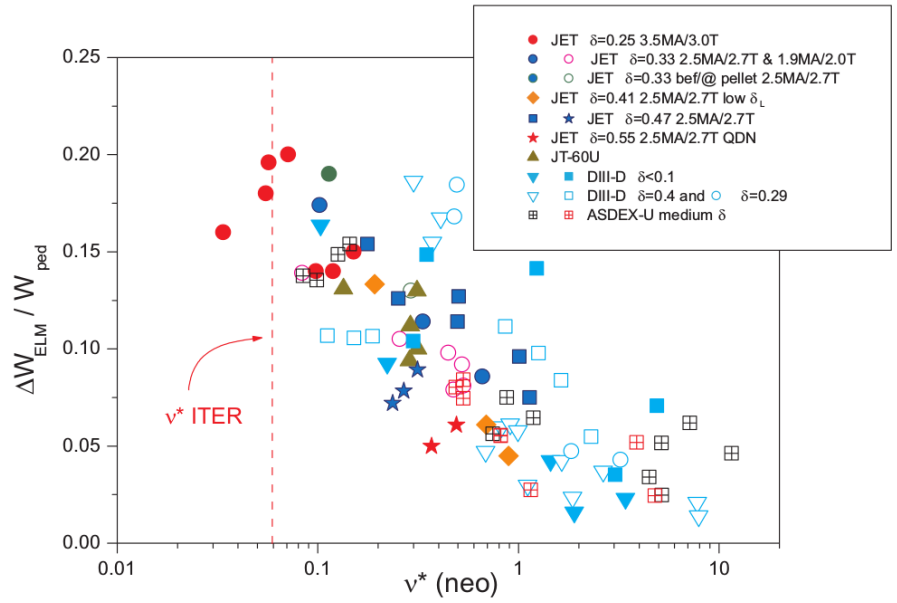

Figure 3.6: The normalised ELM energy loss is plotted against the pedestal plasma collisionality for data points gathered from AUG, DIII-D, JT-60U and JET. Taken from [13].

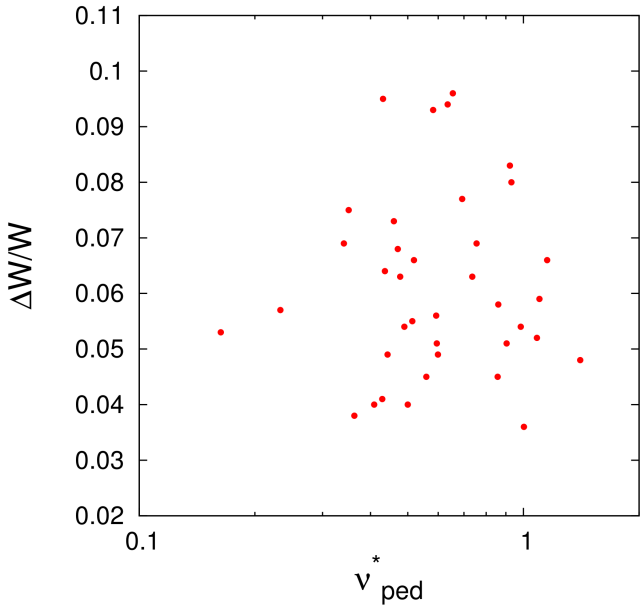

Figure 3.7: The normalised energy loss due to ELMs is plotted versus the dimensionless collisionality ν^*_{ped}.

whilst covering a banana orbit[1]. The energy drop during an ELM may be linked to both a drop in temperature as well as a drop in density. As for the case of densitiy, higher collisionality leads to a smaller drop in temperature during an ELM whereas the density drop seems to stay constant with increasing collisionality [12].

Despite the fact that energy losses depend on plasma parameters, this seems not to be the case for particle losses [13].

It has been shown [13] that the ELM power flux pulse onto the divertor plates is not associated with the duration of the MHD activity, as it was believed earlier, but with the ion parallel transport duration along the magnetic field lines.

3.2.2 Extrapolation to ITER

The fact that there is no valid physical model which is able to fully describe ELMs or the energy transport to the divertor plates during the ELM yet, leads to a

[1]Describes the trajectory of the movement of plasma particles, which are trapped in the outer plasma region due to the magnetic mirroring effect.

problem for extrapolation of the experimental results to ITER. Two approaches are proposed in [13]:

- As shown in figure 3.6, $\nu^* ped$ correlates with the ELM energy loss and it is assumed that extrapolation to ITER is legitimate.
- The parallel ion transport time of the ELM loss energy to the divertor $\tau_{\parallel}^{Front}$ is observed to vary with pedestal plasma parameters. [7] assumes that the energy losses are determined by $\tau_{\parallel}^{Front}$ and the time of enhanced cross field transport τ_{ELM}. In this model the relation $\tau_{\parallel}^{Front} >> \tau_{ELM}$ is valid. The MHD activity during an ELM leads to a connection of the magnetic field lines with the divertor target plates. A variation of ν_{ped}^* leaves the duration of this connection τ_{ELM}^{MHD} unchanged [12]. This is not the case for $\tau_{\parallel}^{Front}$, where we can see a positive correlation, which leaves us with problems in interpreting the results.

There are crucial differences to ITER between those models:

If $\tau_{\parallel}^{Front}$ were to govern the ELM energy loss, the divertor plates would have to withstand energies of about 5-11MJ, which leads to an acceptable lifetime. Whereas if ν_{ped}^* controlled the ELM energy loss, 22 MJ would have to be expected which would lead to unacceptable lifetimes [13].

3.3 Scaling Laws

The physics behind parameters like ELM losses or the ELM frequency is not yet fully understood. Approximations of the dependencies of these parameters are one important step of getting to the bottom of the physical processes.

Empirically found scaling laws are crucial for the prediction of the performance and limits of new fusion devices. They also allow comparisions of the performance of different machines. Scaling laws are produced using large amounts of experimental data preferably from different devices. In this thesis, the generation of scaling laws was performed using a database approach which will be explained in section 4.4. The range of data was limited to results from ASDEX Upgrade

discharges.

Due to its impact on the ignition in the Lawson criterion, the scaling of the energy confinement is of great importance. The ITER physics basis IPB98(y,2) scaling of the energy confinement time in engineering parameters, which is widely accepted, reads as follows [17]:

$$\tau_{E,IPB(y,2)} = 0.0562 \cdot I_p^{0.93} \cdot B_t^{0.15} \cdot P_{loss}^{-0.69} \cdot n^{0.41} \cdot R^{1.97} \cdot \kappa^{0.78} \cdot \epsilon^{0.58} \cdot M^{0.19} \ . \quad (3.6)$$

I_p is the plasma current, B_t is the toroidal magnetic field at the major radius R, P_{loss} is the input power minus the power lost due to radiation and conduction, n is the line averaged density, R is the major radius, κ is the elongation (b/a, where b is the height of the plasma measured from the equatorial plane), ϵ is the inverse aspect ratio (a/R) and M is the average ion mass.

Ryter et al. ([21]) find interesting scaling relations for the thermal confinement time

$$\tau_{th} = \frac{W_{th}}{P_{heat} - dW/dt} \ , \quad (3.7)$$

W_{th} being the plasma energy without the contribution of NBI fast ions. Contrary to equation 3.6, the scaling shows a negative dependence of the line averaged electron density $\bar{n}_e$ and reads

$$\tau_{th} \propto I_p^{1.32} P_{heat}^{-0.72} \delta^{0.31} \bar{n}_e^{-0.18} \quad (3.8)$$

with δ being the triangularity which describes the shaping of a tokamak plasma (see subsection 4.4.2). [21] mentions the often observed case of increasing natural density with an increase of τ_{th} and a reduction of the ELM frequency in the low density range without gas puffing. This low density range is indicated with a ratio between the electron density $\bar{n}_e$ and the Greenwald density limit ([6])

$$n_{GW} = \frac{I_p}{\pi a^2} \quad (3.9)$$

of roughly 0.6. In this density range one therefore finds a positive correlation between $\bar{n}_e$ and τ_{th}.

A second scaling in Ryter et al., which includes the central electron density $n_e(0)$ and the electron density in the scrape-off layer, which was averaged over 6 cm starting from the separatrix outwards and which indicates gas puffing, reads as follows [21]:

$$\tau_{th} \propto I_p^{1.0} P_{heat}^{-0.56} \delta^{0.2} n_e(0)^{0.3} n_{e,SOL}^{-0.17} \ . \tag{3.10}$$

It shows the impact the SOL density has on the confinement time as well as on the core density and for this reason n_{SOL} is included in the scalings in chapter 5.

3.4 High Field Side High Density Front

The high field side high density front (HFSHD) is a region of increased density in the lower scrape-off layer on the inner, high field side of the tokamak vessel. It is an important parameter when it comes to linking fuelling and seeding effects on SOL parameters like the density. Dunne et al. present findings at ASDEX Upgrade which show the impacts of the HFSHD on the pedestal density ([1]).

Neutral fuelling increases the HFSHD density which then causes the radial position of the pedestal density top to radially shift outwards due to an "increase of diffusive and drift driven fuelling of the plasma" ([1]). Nitrogen seeding counteracts this effect shifting the density profile inwards again.

This shows the importance of including the SOL density in the energy confinement time scalings due to its effect on pedestal top parameters.

Chapter 4

Analysis Method

4.1 Diagnostics

During operation of the tokamak, the accessibility of the plasma region with diagnostics is very limited. High magnetic fields and high temperatures make it impossible to install diagnostics inside of the SOL. This makes it a difficult task to measure the plasma parameters. Measurement positions can generally not be varied during a discharge and the diagnostics can therefore only measure along a line of sight. Especially in the edge region, where ELMs occur, a high spatial as well as temporal resolution is needed in order to get satisfying results.

At ASDEX Upgrade a broad range of diagnostic devices is installed to measure the electron temperature and density. Figures 4.1 and 4.2 show where the measurement devices are located in the reactor vessel.

4.1.1 Electron Cyclotron Emission (ECE) Radiometry

ECE radiometry is a method to find the temperature of electrons in a plasma. Electrons, which travel perpendicularly to the magnetic field lines are forced onto a gyration orbit by the Lorentz force. This acceleration leads to a cyclotron radiation which can be measured optically from outside of the plasma. The gyrofrequency is

$$\omega = \frac{neB}{m_e}, \tag{4.1}$$

where n is the integer which denotes harmonics, e is the elementary charge, B is the absolute value of the magnetic field and m_e is the electron mass. In a Tokamak

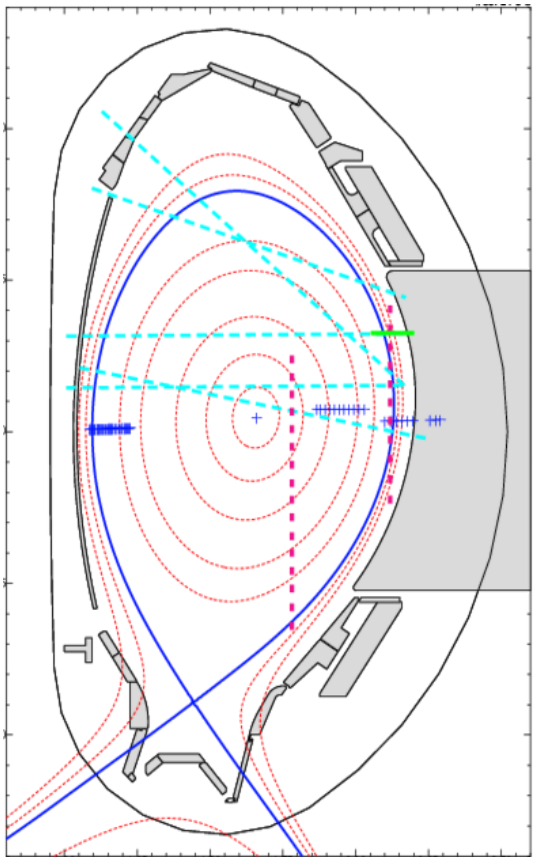

Figure 4.1: Poloidal cross section of the ASDEX Upgrade tokamak vessel and the location of the relevant diagnostics for discharge #33724. The lithium beam is displayed in green, the ECE Radiometer is displayed as blue crosses, the Vertical Thomson Scattering is displayed in pink, the lithium beam is displayed in green and the DCN Interferometer is displayed in light blue. Also, the separatrix (dark blue) and the magnetic flux surfaces (red) are displayed.

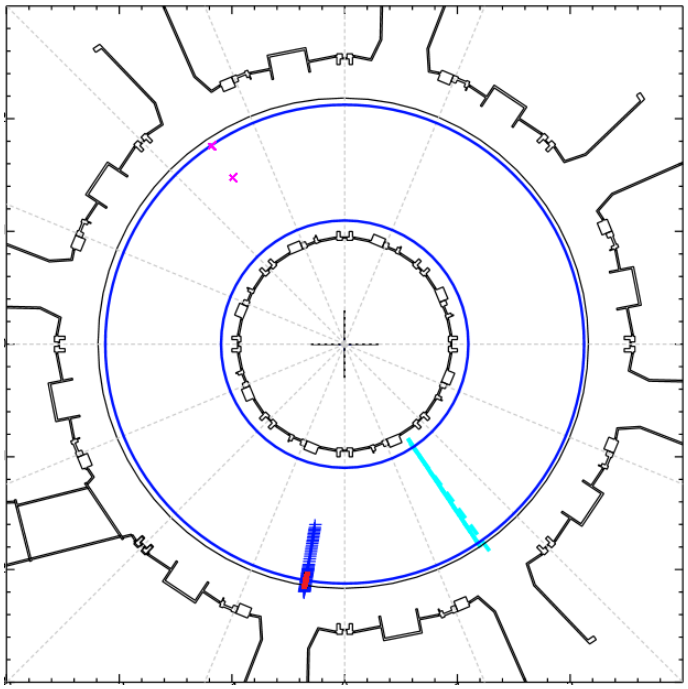

Figure 4.2: Location of the relevant diagnostics in the toroidal cross section view of ASDEX Upgrade for discharge #33724. The ECE Radiometer is displayed as blue crosses, the Vertical Thomson Scattering is displayed in pink, the lithium beam is displayed in red and the DCN Interferometer is displayed in light blue.

the magnetic field (and therefore the gyrofrequency) is inversely proportional to the radius. This relation makes it possible to evaluate the location of the radiation emitted at a particular frequency whose intensity relates to the electron temperature. The B-fields which are typically used in Tokamak devices lead to cyclotron emission wavelenghts at the millimeter scale at which the Rayleigh-Jeans law[1] applies [30]. In the case of an optically thick[2] harmonic the intensity of the radiation is:

$$I_n(\omega) = \frac{\omega^2 T_e(R)}{8\pi^3 c^2}. \tag{4.2}$$

Combinding equation 4.2 and the relation between ω and R makes it possible to measure and localise T_e. One has to be careful analysing data points measured with the ECE radiometry close to the separatrix because of the shine-through effect. In the low density region the measured emission of radiation artificially rises again. This radiation may have contributions from several plasma regions [18].

[1]The Rayleigh-Jeans law gives a relation between the spectral radiance M, the temperature T and the wavelength of the radiation λ: $M \cdot d\lambda = \frac{2\pi c k_B T}{\lambda^4} \cdot d\lambda$

[2]sufficiently high density and temperature

4.1.2 Thomson Scattering

This method uses the scattering of photons (laser beam) from electrons (plasma) to measure the electron temperature. The broadening of the laser spectrum is an indicator for increasing electron temperature. The electron density can also be quantified from an intensity analysis since a high density leads to more scattering and thus a higher intensity of scattered light. The Nd:YAG laser's energy at ASDEX Upgrade is about 1 J, the pulse length is 15 ns and it can be operated in 100 µs intervals [25].

4.1.3 Lithium-Beam Diagnostic

This active diagnostic using a high energy beam of Lithium atoms can be used to measure the electron density in a Tokamak plasma. The neutral atoms are being raised into an excited state or are ionized due to the interaction with the plasma. Relaxation into lower energy states leads to characteristic radiation. This line radiation's intensity depends on the electron density.

If the electron densities are low (up to $4 \times 10^{19}\,\mathrm{m}^{-3}$) an acceptable measurement can be performed up to $\sim 10\,\mathrm{cm}$ from the separatrix which corresponds to $\rho \sim 0.85$ [25].

4.1.4 Interferometry

The phase of a laser beam shifts with increasing distance travelled in plasma with respect to vacuum. From this phase shift the line integrated electron density along the "line of sight" of the laser beam can be evaluated. At ASDEX Upgrade this task is performed by a deuterium cyanide (DCN) laser. The sampling rate of this measurement device is up to 20 kHz [25].

4.2 Equilibrium Reconstruction

In ideal magnetohydrodynamics(MHD), the equilibrium equation for a two dimensional plasma is called the Grad-Shafranov equation. This nonlinear, elliptic partial differential equation can be used to compute the two dimensional

plasma equilibrium in a tokamak assuming toroidal symmetry. For profile analysis, "generic" equilibria are used which are based on magnetic measurements but more sophisticated equilibria exist which include kinetic profiles.

It is crucial to know the exact location of the magnetic flux surfaces in the vessel to be able to combine measurements from diagnostics which are located at different points in the machine. Codes that are able to reconstruct equilibria are for example CLISTE [14] or EFIT [10].

4.3 AUG Pedestal Fitting

The data from each shot at ASDEX Upgrade including the measurements of all diagnostics are written into so called shotfiles. This raw data can be displayed and analysed with a software called *AUG Pedestal Fitting* or short: *augped*. For the data analysis in this thesis, version 2.10 was used.

The region of interest - the pedestal region - is small compared to the dimensions of the total plasma region. Due to limited radial measurement locations only few data points are available which leads to measurement uncertainties. A solution to this problem is to move the plasma slightly outwards in order to create virtual lines of sight. This plasma shift is called an R_{aus} scan. Using different diagnostics results in a large amount of data which will be combined to reduce uncertainties.

Looking at temporal restrictions, gathering data is possible according to a measurement rate which differs from instrument to instrument. In order to increase the amount of data, the quasi-periodicity of ELMs can be used. Over a time period in which the main plasma and engineering parameters are constant it is possible to look at many ELM crashes at a time. Assembling these data points requires averaging over similar events, which has to be done with respect to a certain benchmark. This is done in the ELM synchronisation process (see subsection 4.3.1), which finds the starting time values of each ELM crash through the measurement of the divertor current peaks (see figure 3.2) and reduces the uncertainties in the data.

The next step after synchronising all the data is fitting the data with one of several functions offered by *augped* (see subsection 4.3.2). The fitted values describe the temperature and density profiles and will play a major role in the construction of the pedestal database.

Depending on the shotnumber, different diagnostics are available to perform the fits. Amongst these are (see section 4.1):

- Core Thomson scattering (T_e+n_e)
- Edge Thomson scattering (T_e+n_e)
- ECE Radiometer (T_e)
- New Lithium beam (n_e)
- Interferometers (n_e)

In order for the measurements to overlap and thus to give accurate datapoints for the fit, shifts have to be performed manually (see subsection 4.3.3).

4.3.1 ELM Synchronisation

Seperating pre-ELM profiles from post-ELM profiles is essential for this thesis. In order to compare measurements with respect to an ELM and to increase the amount of available data in the pedestal building process, ELM synchronisation has to be performed. As the name anticipates, this action synchronises data with respect to the starting times of ELMs.

Large uncertainties for a single ELM would give rise to large uncertainties in the derived pedestal properties. Without ELM synchronisation those uncertainties in the data would make it impossible to determine accurate pedestal values from the profile. Data points which do not lie within a certain time interval with respect to the corresponding ELM are not taken into account and therefore a construction of pre and post-ELM pedestal profiles is possible. In this thesis, the time intervals out of which data was taken from were chosen manually. For generating pre-ELM electron temperature and density profiles the intervals had a magnitude of 2 ms. The interval for post-ELM profiles was 1.25 ms.

Using the ELM synchronisation method, one has to make sure that the profiles have to be recurrent, so they do not vary strongly from ELM to ELM. This behaviour can be expected when, for unvaried global plasma parameters, the ELM characteristics do not change significantly [25].

4.3.2 Fit Functions/Fitting Procedure

A pedestal can be described by its top value, its gradient and the radial width of the region between top value and the pedestal minimum. Since there is no universally valid definition of the pedestal top, one has to choose a definition which is consistent with all other data used as well as with the definition in the used literature. A more practical description says that the pedestal top value is in the transition region from steep gradient to flat gradient.

There are different mathematical models that can be used to find the different pedestal values. The two-line-method for example defines the pedestal top as intersection between two lines that are fitted to the data points. This bilinear fit represents the region of a steep gradient and the region with a flat gradient inside the pedestal top, which holds only in the region close to the pedestal top value.

In this thesis the mtanh[3]-method was used to find the pedestal values. The advantage over the two-line-method is its smoothness and flexibility. A hyperbolic tangent is used which has been modified using polynomials in order to meet the needs of connecting the core region with the edge region. The function is plotted in figure 4.3. Similarly to the two-line-method, the result is deteriorated if the data is fitted over the whole normalized radius. In this thesis, fits have mostly been performed across a range between $\rho = 0.8$ and 1.1. The quality and suitability of the different fitting methods were tested in [25]. Both methods can be used for fitting the pedestal top, but large errors would result in the computation of the ELM affected area using a two-line fit.

[3]Modified hyperbolic tangent

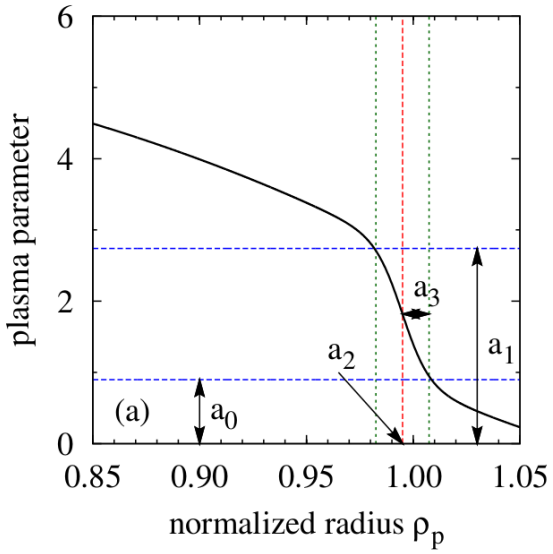

Figure 4.3: Modified hyperbolic tangent representing a typical plasma parameter (e.g. electron temperature) profile in H-mode. a_0 represents the offset, a_1 the pedestal top value, a_2 the symmetry radius and a_3 the half width. Taken from [25].

4.3.3 Shifting the Data

One diagnostic is insufficient to build a pedestal profile and therefore a combination of measurement points from different diagnostics has to be used (see section 4.3). As shown in figures 4.1 and 4.2, the diagnostics are located at different toroidal and poloidal locations in the torus. When the results are mapped onto a common axis using the normalised radius ρ as a radial coordinate, a radial displacement of the data points can occur. In order to remove this error in the conversion from raw measurement data to the displayed values, a shift of up to 2 cm has to be performed manually. Otherwise the displayed measurements would not correspond to the real data values which have been measured by the instruments. Possible sources for this error are [25]:

- "Uncertainties in the determination of the observation volumes in machine coordinates."

- Deviation of the toroidal symmetry. The data might be accurate but due to toroidally non-symmetric profiles the data does not overlap. It is not very probable that this error source is able to describe shifts of this magnitude, but a shift of about 5 mm has been measured at AUG [4].

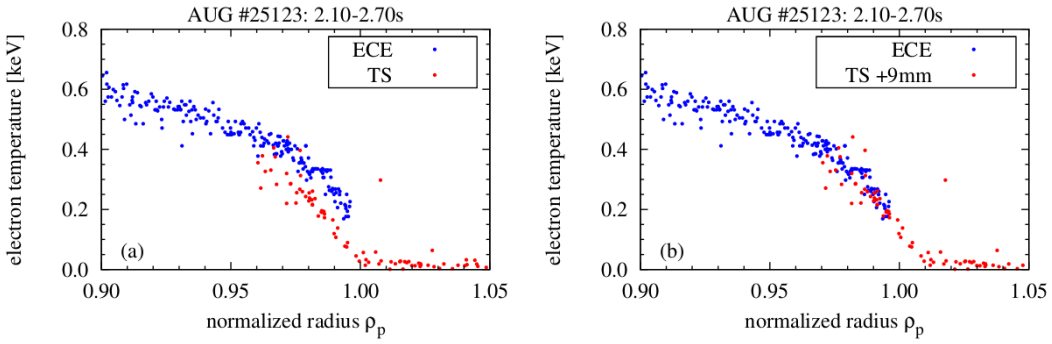

Figure 4.4: Alignment of ECE and TS. A TS diagnostic shift of 9mm was performed in (b) contrary to (a).

- Inaccuracy in the equilibrium reconstruction. An uncertainty of the separatrix position above the midplane hinders an accurate combination of the data points.

Under the assumption that the heat flux which is coming out of the plasma does not dissipate, the temperature at the divertor target plates will determine the temperature of the separatrix. The separatrix temperature at ASDEX Upgrade is approximately 100 eV and gives the absolute location of the TS diagnostic shift. After the TS shift, the ECE will be shifted correspondingly. For the electron density, the same TS shift is performed and the lithium beam shift is adjusted to the TS values.

A shift of the TS diagnostic for better alignment is shown in figure 4.4.

4.3.4 Pedestal Top Values

Since the evaluation of the pedestal top values using the mtanh-fit and the *read_pedestal* routine, which finds all relevant pedestal parameters from the fitted functions, is empirically inaccurate and computes a non-intuitive pedestal top, a modification to these values had to be performed.

In order to counteract the tendency of the modified tanh to fit the pedestal top too far in the steep pedestal gradient region, the radial value of the pedestal center (a2 in figure 4.3) was subtracted with 1.5 times the half width (a3) of the pedestal resulting in the radial value of the new pedestal top. The new pedestal top is now in a region of a flat gradient leading to less uncertainties. It is important that these calculations are performed consistently in all fits.

4.4 Database

It is important to determine physical dependencies between parameters that are used in a scaling. Finding such correlations can be done in several ways. The most direct approach is to vary one specific parameter whilst keeping all other parameters unchanged. Especially at tokamak experiments these parameter scans require an enourmous amount of experimental time which increases significantly if one wants to add more parameters to the process of finding parameter correlations. Using this method, the relations between the remaining unchanged parameters stay unknown.

In this thesis a database was built in order to find dependencies between a large number of parameters, namely discharge settings, plasma properties and dimensionless parameters. This approach has the advantage of using the available data very efficiently. Including more shots to the database provides a broader data range. Excluding shots from the database may lead to better understanding of relations between a smaller set of parameters if a reduction of variation of certain parameters is achieved. For example, one parameter can be left constant over all shots.

But the database approach also comes along with disadvantages. There might be no physical reason to include a parameter from the database in a scaling leading to a distortion of the exponents. Another problem arises if a parameter which is constant in the database is included in the scaling. Not all shots have to follow the trend given by the correlation values. Statistical effects or incomplete models can affect the results in a negative way and thus, a lot of data has to be used in order to reduce these errors.

4.4.1 Used Data

Table 4.1 lists all the shots and time intervals that were used in this thesis.

shot number	time interval [s]
23418	2.700 - 2.850
23418	2.285 - 3.000
23418	3.150 - 3.300
23418	3.000 - 3.150
24148	2.200 - 2.350
24148	2.350 - 2.500
24148	2.500 - 2.650
26313	2.600 - 3.400
26313	6.000 - 6.600
26466	2.000 - 2.400
30411	4.500 - 4.700
30411	2.800 - 3.000
30889	3.200 - 3.500
30889	4.300 - 4.500
30890	3.300 - 3.500
30890	4.300 - 4.500
30891	3.300 - 3.500
30891	4.300 - 4.500
30891	5.300 - 5.500
30892	3.300 - 3.500
30892	4.300 - 4.500
30892	5.300 - 5.500
30899	3.100 - 3.400
30899	4.100 - 4.400
30900	3.300 - 3.600
30900	4.900 - 5.200
30901	2.800 - 3.000
30901	4.300 - 4.600
32201	2.800 - 3.000
32201	3.600 - 3.800
32201	4.800 - 5.000
32201	5.600 - 5.800
32930	2.650 - 2.850
32931	2.800 - 3.000
32932	2.750 - 2.950
32950	2.750 - 2.950
32953	2.800 - 3.000
32953	3.800 - 4.000

Table 4.1: Table listing all shots and time intervals included in the database.

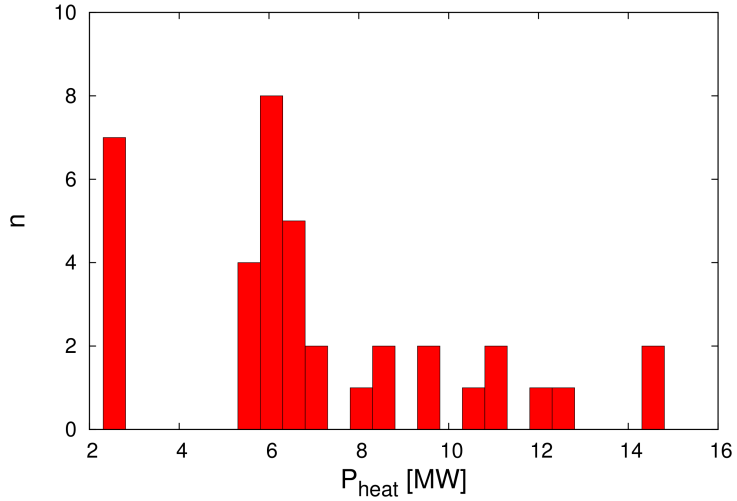

Figure 4.5: Analysed data range of P_{heat} versus the abundance of the values.

4.4.2 Used Parameters

ELM energy losses depend on the edge pedestal plasma parameters before the start of the ELM. As shown in 3.2.1, the plasma collisionality, for example, is believed to be a very important one but we have already shown that this dependence was not found in the ASDEX Upgrade data used in this thesis (figure 3.7). Yet, it seems to be a good ordering parameter when comparing data across many different Tokamaks [13].

According to the literature (e.g. [12], [13]), many parameters seem to have a direct or an indirect impact on ELM losses. Some of them are listed below:

- heating power P_{heat} (see figure 4.5).
- plasma current I_p. Discharges with 0.6, 0.8, 1.0 and 1.1 MA were analysed (see figure 4.6).
- toroidal magnetic field B_t. Values between 1.94 T and 2.78 T were analysed(see figure 4.7).
- electron pedestal temperature T_{ped}
- electron pedestal density n_{ped}
- electron SOL density n_{SOL}

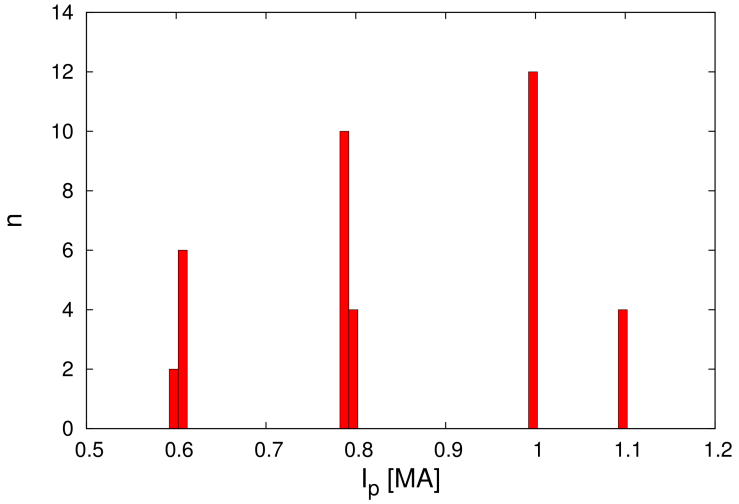

Figure 4.6: Analysed data range of I_p versus the abundance of the values.

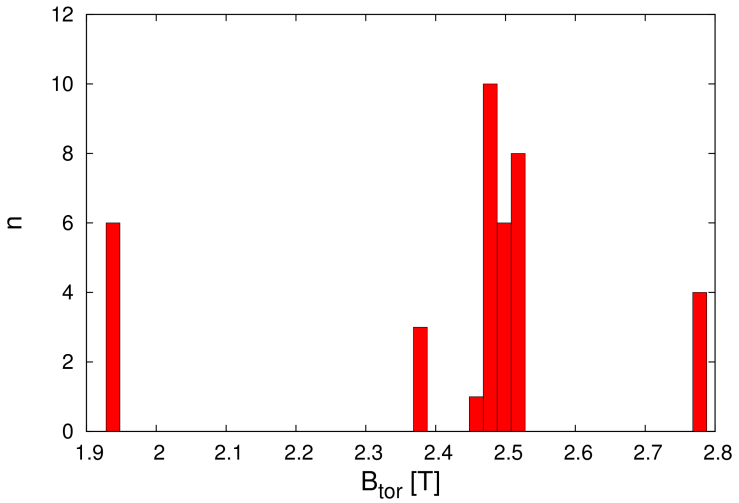

Figure 4.7: Analysed data range of B_{tor} versus the abundance of the values.

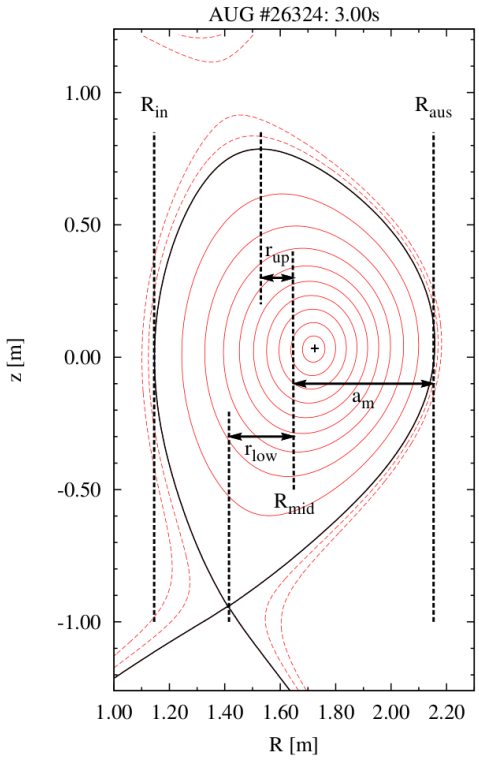

Figure 4.8: Parameters which determine the triangularity in the poloidal cross section of the vessel. Taken from [25].

- divertor density n_{div}
- collisionality ν^*_{ped}
- parallel transport time $\tau_{\parallel}^{Front}$, which is defined as

$$\tau_{\parallel}^{Front} = (1 + \sqrt{3/2} \cdot \nu^*_{ped}) \frac{2\pi \cdot R \cdot q_{95}}{c_{sound}} \quad . \tag{4.3}$$

- safety factor q_{95}, which gives the number of poloidal orbits of a magnetic field line per toroidal orbit measured at 95% of the flux.
- electron density normalised to Greenwald limit n/n_{GW}
- ELM frequency f_{ELM}

[12] shows that ELM losses have a strong dependence on the triangularity δ, which is computed as $\frac{\delta_{low}+\delta_{up}}{2}$, where δ_{low} and δ_{up} are normalised deviations from

an ellipse, s. The upper and lower triangularity (see figure 4.8) are defined as

$$\delta_{low,up} = \frac{r_{low,up}}{a_m} \quad . \tag{4.4}$$

Inspite of this, the triangularity was not used in this thesis due to the fact that it was not varied in the data set and is therefore not includable.

Many of them have been chosen for comparison but have been dropped in this thesis due to insufficient gain. These include $\tau_{\parallel}^{Front}$, n/n_{GW}.

Parameters which have also not been looked at in this thesis are for example the gas fuelling rate, the parameter for plasma performance

$$\beta = \frac{p_{ped}}{(\langle B_p \rangle^2 + B_t^2)/(2\mu_0)} \tag{4.5}$$

or the ratio of the Larmor radius to a normalizing length scale

$$\rho^* = \frac{\rho_{i,L}}{a} = \frac{m_i v_\perp}{a q_i B_t} \quad . \tag{4.6}$$

4.4.3 Computing W_{MHD}^{pe}

It is possible to compute the value of W_{MHD} by integrating the pressure, which is the product of the density and the temperature, over the volume:

$$W_{MHD}^{pe} = \frac{3}{2} \int p dV \tag{4.7}$$

Using these values for the pedestal stored energy, the size of the stored energy losses in the pedestal due to ELMs were calculated and compared to the overall losses.

It is important to notice that in this calculation only electron values were used. High scatter can be seen (figure 4.9) comparing ΔW_{MHD}^{pe} and ΔW_{MHD}^{GQH}, the latter being obtained using W_{MHD} values from the GQH equilibrium reconstruction. Due to these uncertainties which result from large variations in the ELM-affected area of the fitted profiles, ΔW_{MHD}^{GQH} was used throughout this thesis being a more reliable measurement.

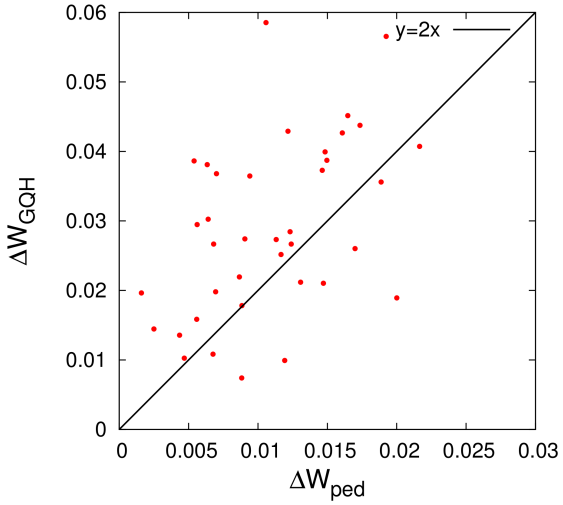

Figure 4.9: Energy loss due to ELMs obtained from the equilibrium reconstruction plotted against the same value obtained from computing equation 4.7.

4.4.4 Data Regression

Due to the chosen database approach in this thesis uncertainties concerning which parameters influence a specific variable arise. Getting rid of unnecessary parameters is therefore essential for the creation of a scaling law. In this thesis a log-linear data regression was used to find correlations between the energy confinement time τ_E and the other parameters included in the database.

A power law approach for the set of equations

$$q_i = c \cdot \prod_{j=0}^{n} p_{i,j}^{a_j}, \tag{4.8}$$

where c is a constant, p is a parameter and a the corresponding exponent. Using the logarithmic function on equation 4.8 gives a set of linear equations, namely:

$$\ln q_i = \ln c + \sum_{j=0}^{n} a_j \ln p_{i,j}, \tag{4.9}$$

which are now solvable using a regression algorithm.

The root mean squared error (RMSE) is a useful quantity when it comes to evaluating the quality of a scaling law since it shows how much the experimental

results $t_i^{(exp)}$ differ from the modelled values of the scaling law $t_i^{(scal)}$.

$$\mathrm{RMSE}(\%) \coloneqq 100 \cdot \sqrt{\frac{1}{N-1}\sum_{i=1}^{m}(\ln q_i^{(exp)} - \ln q_i^{(scal)})^2} \tag{4.10}$$

The smaller the value of RMSE the more accurate is the model. If an additional parameter does not change the RMSE or increases it, it should be neglected for the model. Correlated parameters can be a problem for the accuracy of the exponentials. If a parameter is added and the exponentials change significantly even though the RMSE does not, the parameter is probably strongly correlated to another one. To find these dependencies the use of parameters should be alternated in the regression [25].

4.4.5 Parameter Correlations

Prior to constructing scaling laws using a regression method, one should evaluate dependencies between the parameters which are included in the database (see section 4.4.5). As previously discussed, the parameters can be divided in subgroups (see section 4.4.2). The discharge settings and the plasma parameters can be combined under the term engineering parameters, which we will look at now.

The plasma current I_p is rather strongly correlated to both heating power P_{heat} and toroidal field B_{tor} as can be seen in table 5.1. However the highest correlation of I_p is the one it has to the electron density n_{ped}[4]. These high positive correlations can have two origins. Either they are due to a physical interdependence or due to operational limits of the Tokamak. An example for the latter would be a case in which a parameter can only be raised to a certain level in an experiment if another (non-physically) dependent parameter has a minimal value. Since the analysis convers many shots over a broad range of parameter values in the database approach such dependencies are inevitable.

It is crucial to figure out whether some correlations are only given because certain parameter variations were omitted in the process of selecting data. Thus, shots from different parameter scans were included into the database. Correla-

[4]In chapter 5, where the results are presented this dependence will be adressed again.

tions will be discussed in the next chapter, where also examples will be shown.

Chapter 5

Results

Using a regression function scaling laws were computed for the energy confinement time as well as for the power loss due to ELMs. It was checked whether the substitution of P_{heat} with $P_{reduced}$ leads to better scalings or not. In this context, the reduced heating power is defined as

$$P_{reduced} = P_{heat} - P_{ELM} \quad , \tag{5.1}$$

with P_{ELM} being the power lost due to ELMs. This parameter is defined as

$$P_{ELM} = \Delta W_{MHD}^{GQH} \cdot f_{ELM} \quad . \tag{5.2}$$

In this equation f_{ELM} is the ELM frequency. For better readability "GQH" will be omitted from ΔW_{MHD}^{GQH} in all following equations.

The results of this endeavour will be presented in this chapter.

5.1 Parameter Correlations

As mentioned in subsection 4.4.5, strongly correlating parameters are tricky for scaling laws. Those parameters scale similarly and if they are included in the same scaling they will influence each other so that it remains unclear which parameter is the most physically relevant.

In order to get an overview over the parameter correlations, a correlation

matrix (see table 5.1) was created using linear Pearson correlation coefficients (PCC).

The PCC values have the following meaning:

$$PCC = \begin{cases} 1 \rightarrow \text{total positive correlation} \\ 0 \rightarrow \text{no correlation} \\ -1 \rightarrow \text{total negative correlation} \end{cases} \tag{5.3}$$

	I_p	B_t	P_{heat}	P_{ELM}	$P_{reduced}$	n_{ped}	n_{div}	n_{SOL}
I_p	1	0.709	0.675	0.566	0.610	0.826	0.627	0.415
B_t	0.709	1	0.495	0.344	0.528	0.491	0.300	0.469
P_{heat}	0.675	0.495	1	0.887	0.847	0.528	0.549	0.589
P_{ELM}	0.566	0.344	0.887	1	0.507	0.402	0.533	0.568
$P_{reduced}$	0.610	0.528	0.847	0.507	1	0.523	0.412	0.447
n_{ped}	0.826	0.491	0.528	0.402	0.523	1	0.813	0.587
n_{div}	0.627	0.300	0.549	0.533	0.412	0.813	1	0.704
n_{SOL}	0.415	0.469	0.589	0.568	0.447	0.587	0.704	1

Table 5.1: Correlation Matrix computed using an IDL routine.

Strong correlations are found between n_{div} and the pedestal density n_{ped}, $P_{reduced}$ and P_{heat}, P_{ELM} and P_{heat}, n_{ped} and I_p as well as B_t and I_p. At this point it has to be mentioned that the correlations do not necessarily indicate a physical dependence since one also has to take into account operational constraints on engineering parameters.

5.2 Scaling Laws for τ_E

Equation 3.6 showed the IPB98(y,2) scaling for the energy confinement time. In order to verify this equation for ASDEX Upgrade data the same parameters ought to be used in the new scaling law. The major radius R and the inverse aspect ratio ϵ cannot be varied at ASDEX Upgrade and the elongation κ as well as the fuel mass M were not changed in the used data set. A scaling for the leftover parameters I_p, B_t, P_{heat} and n_{ped} is shown below:

$$\tau_E = const. \cdot I_p^{1.04(\pm 0.35)} \cdot B_t^{-0.36(\pm 0.39)} \cdot P_{heat}^{-0.52(\pm 0.09)} \cdot n_{ped}^{-0.09(\pm 0.14)} \ , \tag{5.4}$$

with a RMSE of 7.96. If compared to equation 3.6, one finds a similar dependence of τ_E on the plasma current and on the input power. The other two parameters do not seem to fit the energy confinement time well and are therefore omitted from the scaling step by step to see how the RMSE changes. The scalings below use all data which was included in the database. The obtained equations read

$$\tau_E = const. \cdot I_p^{0.87(\pm 0.23)} \cdot B_t^{-0.22(\pm 0.33)} \cdot P_{heat}^{-0.52(\pm 0.09)} \quad (\text{RMSE} = 7.77), \tag{5.5}$$

$$\tau_E = const. \cdot I_p^{0.83(\pm 0.26)} \cdot P_{heat}^{-0.54(\pm 0.08)} \cdot n_{ped}^{-0.03(\pm 0.12)} \quad (\text{RMSE} = 7.65) \tag{5.6}$$

and

$$\tau_E = const. \cdot I_p^{0.79(\pm 0.20)} \cdot P_{heat}^{-0.54(\pm 0.08)} \quad (\text{RMSE} = 7.65). \tag{5.7}$$

The scaling law 5.7 will from now on be denoted as the τ_{MM}-scaling in this thesis.

Using the ELM-reduced heating power $P_{reduced}$ instead of P_{heat} results in

$$\tau_E = const. \cdot I_p^{0.30(\pm 0.22)} \cdot P_{reduced}^{-0.40(\pm 0.07)} \cdot n_{ped}^{0.11(\pm 0.12)} \quad (\text{RMSE} = 11.79) \tag{5.8}$$

and

$$\tau_E = const. \cdot I_p^{0.42(\pm 0.18)} \cdot P_{reduced}^{-0.40(\pm 0.07)} \quad (\text{RMSE} = 11.75), \tag{5.9}$$

where one is able to see a big drop in the I_p exponent and an increased RMSE. This leads to the result that the new scaling is worse than the original one.

We have seen in section 5.1 that I_p and n_{ped} are rather strongly correlated and it is therefore not adviseable to use both parameters in the same scaling. Using the SOL density instead of the pedestal density results in

$$\tau_E = const. \cdot I_p^{0.82(\pm 0.20)} \cdot P_{heat}^{-0.45(\pm 0.09)} \cdot n_{SOL}^{-0.11(\pm 0.07)} \quad (\text{RMSE} = 7.24), \tag{5.10}$$

and

$$\tau_E = const. \cdot I_p^{0.49(\pm 0.18)} \cdot P_{reduced}^{-0.28(\pm 0.09)} \cdot n_{SOL}^{-0.16(\pm 0.07)} \quad (\text{RMSE} = 10.21), \tag{5.11}$$

which also shows the negative influence of using $P_{reduced}$ on the scaling's performance. Equations 5.6 and 5.10 have both very low RMSE values but exchanging

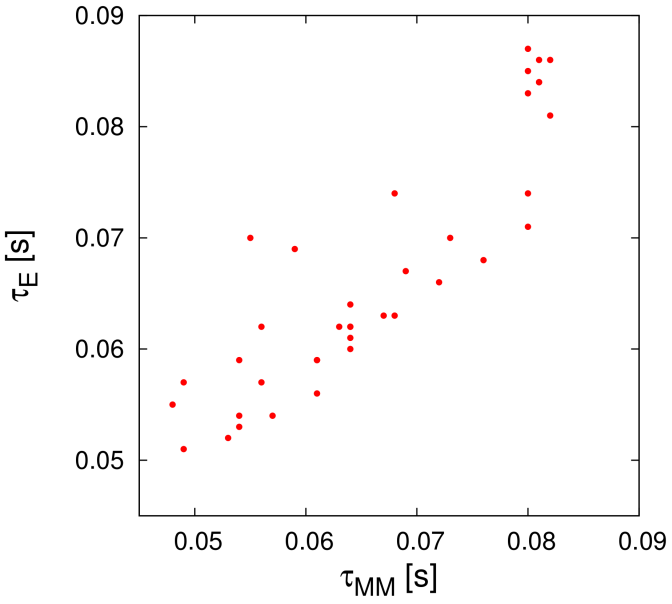

Figure 5.1: Correlation of the confinement time τ_{MM} using the scaling law from equation 5.7 and the actual confinement time from the shotfile τ_E.

the pedestal density for the SOL density seems to alter the heating power's exponent. The RMSE of equation 5.10 is a little lower than the one of the τ_{MM}-scaling but it also has an additional parameter which in addition has only a small impact on the scaling due to its low exponent.

In order to find more information about the large differences of the I_p exponents between the scalings using P_{heat} and $P_{reduced}$ respectively, a smaller data set of 24 timeslices was used in which neither I_p nor B_{tor} was varied. The resulting scalings are shown below.

$$\tau_E = const. \cdot P_{heat}^{-0.31(\pm 0.11)} \quad (\text{RMSE} = 14.12) \tag{5.12}$$

$$\tau_E = const. \cdot P_{reduced}^{-0.14(\pm 0.06)} \quad (\text{RMSE} = 15.08) \tag{5.13}$$

$$\tau_E = const. \cdot P_{heat}^{-0.22(\pm 0.11)} \cdot n_{SOL}^{-0.16(\pm 0.05)} \quad (\text{RMSE} = 10.26) \tag{5.14}$$

$$\tau_E = const. \cdot P_{reduced}^{-0.08(\pm 0.06)} \cdot n_{SOL}^{-0.16(\pm 0.05)} \quad (\text{RMSE} = 12.01) \tag{5.15}$$

These scalings show that in contrast to the scalings resulting from the whole dataset n_{SOL} is important to describe the energy confinement time at constant values of I_p and B_{tor}.

	$H_{IPB(y,2)}$	H_{MM}	$H_{reduced}$
mean:	0.909	1.012	1.021
standard deviation:	0.105	0.082	0.124
used scaling law:	eq. 3.6	eq. 5.7	eq. 5.9

Table 5.2: Results for the calculations of different H-factors.

To conclude the energy confinement time seems to be dominated by the heating power and the poloidal plasma current.

5.3 H-Factor

The quality of the fit can be seen in figure 5.1. This plot leads us to the calculation of the H-factor, which is an important quantity when it comes to valuing the scaling. It is defined as

$$H = \frac{\tau_E}{\tau_{E,scaling}}. \tag{5.16}$$

The H-factor which is normalised to the ITER physics basis IPB98(y,2) scaling will be referred to as $H_{IPB(y,2)}$ in this thesis.

The calculation of the energy confinement time normalised to the scaling τ_{MM} resulted in an H-factor which has a mean of (averaged over all shots) which is closer to 1 than the mean of $H_{IPB(y,2)}$ (see figure 5.2). Of course, a value close to one was expected for the new scalings since the H-factor is now the fraction of the measured τ_E data over the scaling of the fit of the same data. The standard deviation of the data set using the new scaling law is smaller than the standard deviation using the $\tau_{E,IPB(y,2)}$ scaling. In the case of including the losses due to ELMs one gets a higher standard deviation which represents the worse quality of the scaling obtained (see figure 5.3). The results are displayed in table 5.2.

One may divide figure 5.3 into three bands at $H_{reduced}$ values of 0.8, 1.0 and 1.2 which could be interpreted as a indicator for a missing leading ordering parameter in scaling 5.9. This may be either B_t, or n_{SOL} or some other parameter as neither of these significantly reduced the RMSE.

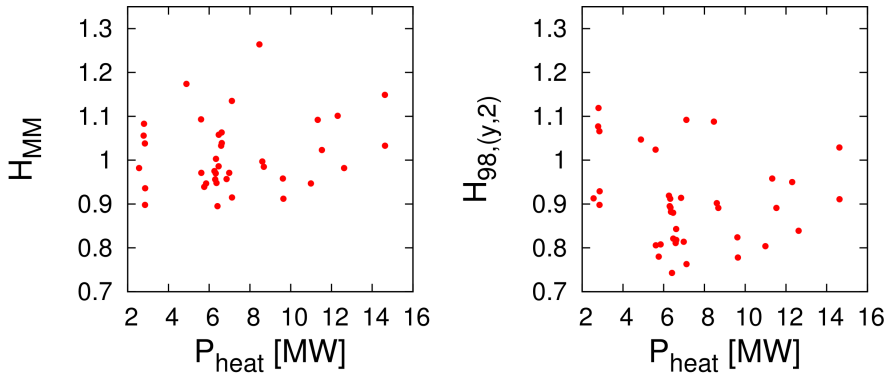

Figure 5.2: Comparision of the H-factor H_{MM}, computed using equation 5.7 to H98(y,2). Both magnitudes are plotted against P_{heat}.

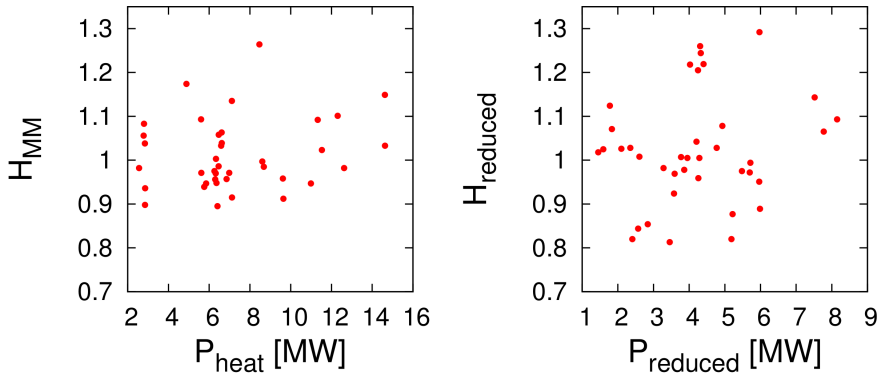

Figure 5.3: Comparision of the H-factor H_{MM}, computed using equation 5.7 and plotted against P_{heat} to the H-factor $H_{reduced}$, computed using equation 5.9 and plotted against $P_{reduced}$.

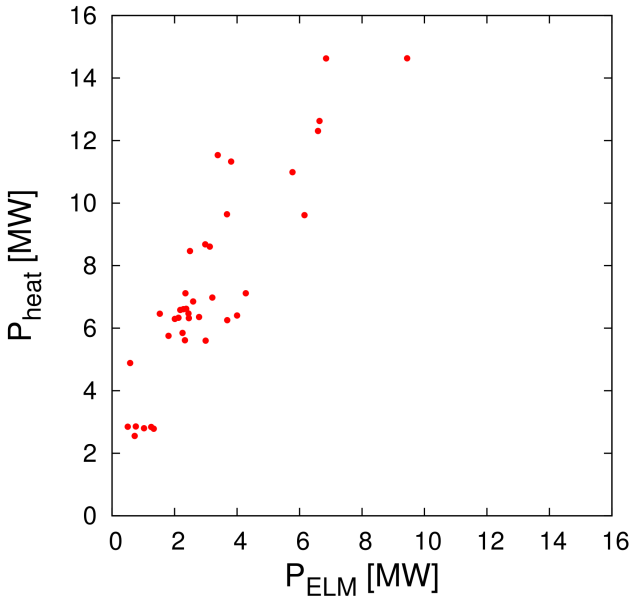

Figure 5.4: Strong correlation between P_{heat} and P_{ELM}

5.4 Ordering Parameter for ELM losses

The power P_{ELM} which gets expelled from the plasma onto the plasma facing components (PFCs) and the divertor due to ELMs cannot easily be described by a scaling law. The reason for this are the components P_{ELM} is made of, namely being the energy lost per ELM ΔW_{MHD} and the ELM frequency f_{ELM}. The ELM frequency is proportional to P_{heat} whereas the dependence of ΔW_{MHD} on P_{heat} is not fully understood yet. [11] observe that there is no dependence between the two latter parameters. For low triangularities the relation

$$f_{ELM} \times \Delta W_{MHD} \sim const. \times P_{heat} \tag{5.17}$$

holds for most discharge settings [12].

Because of the reasons stated above, one has to be careful when creating scaling laws for ELM losses and thus two separate scaling laws for the factors of P_{ELM} were produced.

5.4.1 Scaling for ELM Energy Losses ΔW_{MHD}

In terms of using engineering parameters, plasma current and toroidal magnetic field do not seem to be good parameters to describe ΔW_{MHD} on their own. Figure 5.4 shows the strong correlation between P_{heat} and P_{ELM} which explains why it is problematic to scale ΔW_{MHD} using P_{heat}. A selection of the calculated scalings for the full data set are compactly shown in table 5.3.

ΔW_{MHD}									
T_{ped}	n_{ped}	n_{div}	n_{SOL}	B_{tor}	I_p	q_{95}	ν^*_{ped}	Δt_{ELM}	RMSE
0.61 ±0.26	0.87 ±0.24								33.50
0.66 ±0.26	1.10 ±0.32					0.71 ±0.69			32.98
0.57 ±0.22		0.36 ±0.07							29.87
0.62 ±0.21			0.63 ±0.12						29.25
0.50 ±0.26	0.36 ±0.25		0.52 ±0.14						28.39
				1.75 ±0.76	1.07 ±0.39				31.16
0.70 ±0.77		0.35 ±0.10					0.07 ±0.39		29.85
				1.93 ±0.75	0.83 ±0.41		-0.21 ±0.12		29.84
0.42 ±0.22		0.39 ±0.07						-0.44 ±0.19	27.74
0.48 ±0.19		0.24 ±0.07		1.84 ±0.51					25.34
0.54 ±0.21		0.31 ±0.10		1.64 ±0.56		0.49 ±0.57			26.80
0.38 ±0.20		0.28 ±0.07		1.64 ±0.50				-0.32 ±0.17	24.06
0.38 ±0.20		0.21 ±0.10	0.17 ±0.17	1.46 ±0.53				-0.31 ±0.17	23.72

Table 5.3: Scaling parameters and corresponding exponents. Each row represents a seperate scaling where the parameters have to be multiplied.

Unsatisfactory RMSE values lead to believe that either

- more data samples have to be used to find a satisfactory scaling for the

ELM energy losses or

- the physical process cannot be understood using the parameters shown above.

At low densities, the density pedestal can be described by neutral penetration, which is determined by the divertor density in a first order approximation. More neutral particles and therefore a higher n_{div} value lead to a higher density pedestal. A strong correlation for these parameters was shown in table 5.1. But this relation does not always hold because for higher densities the distribution of neutrals throughout the vacuum vessel also plays a role in the theory. Gas can get trapped in the SOL in which case the density pedestal top does not change. This is the reason for including n_{SOL} in table 5.3.

For a full description the SOL plasma distribution has to be taken into account, but this is still work in progress.

In contrast to [13], where they looked at the dependence of $\frac{\Delta W_{MHD}}{W_{ped}}$ no satisfactory collisionality dependence was found in the ΔW_{MHD} scalings. This might be due to fact that the collisionality range was rather low in the used data set or that another parameter governs the collisionality dependence which has not been included.

It was found that the best scalings can be achieved using the pedestal temperature, the divertor or SOL density and the toroidal magnetic field strength. This shows that the pedestal top and anything connected to B_{tor} seems to be important to describe ELM losses. In addition SOL parameters seem to play a role and should not be omitted in further research as was also shown in [24].

5.4.2 Scaling for ELM Frequency f_{ELM}

The ELM frequency decreases with increasing density, no matter which density is taken into account. It also increases with increasing heating power in any combination of parameters. This is expected since only Type-I ELMs were considered in this thesis. Furthermore, it can be seen clearly that $P_{reduced}$ is not a good scaling parameter for the ELM frequency. The proportionality of the ELM frequency

and the ELM duration Δt_{ELM} is non intuitive and the scaling laws using Δt_{ELM} lead to believe that there could be a physical process linking the two parameters.

The exponent of the plasma current changes dramatically with changing density parameter and was eliminated from the scaling. The exponent of the toroidal magnetic field also does not seem to represent the scaling well since excluding it does not change the RMSE significantly. q_{95} is proportional to $\frac{B_t}{I_p}$ and is therefore a possible source for large changes in the exponents. It seems to be a good scaling parameter if combined with P_{heat} and n_{ped} though, since it lowers the RMSE significantly if added to the scaling law.

f_{ELM}										
T_{ped}	n_{ped}	n_{div}	n_{SOL}	P_{heat}	P_{red}	B_{tor}	I_p	q_{95}	Δt_{ELM}	RMSE
0.03 ±0.25	-0.12 ±0.11							-1.54 ±0.66		32.21
0.48 ±0.21	-0.01 ±0.07								0.88 ±0.18	26.62
		-0.27 ±0.08		0.97 ±0.13		-2.06 ±0.56	0.27 ±0.38			21.09
	-1.05 ±0.21			0.80 ±0.11		-2.37 ±0.49	1.05 ±0.38			18.17
			-0.40 ±0.12	1.04 ±0.14		-1.06 ±0.58	-0.58 ±0.33			20.95
	-0.94 ±0.28			0.67 ±0.10		-1.89 ±0.44	1.04 ±0.34		0.42 ±0.11	15.20
	-1.15 ±0.21			0.70 ±0.12		-0.66 ±1.08	-0.10 ±0.76	-1.60 ±0.91		17.35
	-0.66 ±0.16			0.90 ±0.11		-1.70 ±0.45				19.98
			-0.37 ±0.12	0.90 ±0.12		-1.58 ±0.51				21.93
	-0.55 ±0.16		-0.22 ±0.12	0.98 ±0.11		-1.49 ±0.45				18.93
	-0.55 ±0.14			0.77 ±0.10		-1.22 ±0.42			0.42 ±0.13	17.30
	-1.15 ±0.20			0.70 ±0.11		-0.79 ±0.49		-1.50 ±0.46		17.35
		-0.04 ±0.20			0.47 ±0.19	-0.99 ±0.72				32.06
	-0.44 ±0.24				0.56 ±0.17	-0.83 ±0.69				30.71
			-0.10 ±0.17		0.47 ±0.18	-0.90 ±0.76				31.98
		-0.26 ±0.08		0.74 ±0.13						25.53
	-0.76 ±0.18			0.69 ±0.10						23.73
			-0.47 ±0.13	0.74 ±0.12						24.78
	-0.58 ±0.16			0.59 ±0.09					0.54 ±0.13	19.36
	-1.32 ±0.18			0.58 ±0.08				-1.92 ±0.38		18.03

Table 5.4: Scaling parameters and corresponding exponents. Each row represents a seperate scaling where the parameters have to be multiplied.

Chapter 6

Conclusion and Outlook

In this thesis, scaling laws for the energy confinement time were computed using ASDEX Upgrade data. It was found that using $P_{reduced}$ instead of P_{heat} has no positive effect on the RMSE of the scaling laws for τ_E, ΔW_{MHD} and f_{ELM}. This observation holds for a number of various data sets and additional scaling parameters. The findings were supported by the calculation of the H-factors which show the same trend. Comparing the IPB98(y,2) scaling

$$\tau_{E,IPB(y,2)} = 0.0562 \cdot I_p^{0.93} \cdot B_t^{0.15} \cdot P_{loss}^{-0.69} \cdot n^{0.41} \cdot R^{1.97} \cdot \kappa^{0.78} \cdot \epsilon^{0.58} \cdot M^{0.19} \quad (6.1)$$

to the computed scaling

$$\tau_E = const. \cdot I_p^{0.79(\pm 0.20)} \cdot P_{heat}^{-0.54(\pm 0.08)} \quad (6.2)$$

shows that similar exponents are obtained for the heating power and the poloidal plasma current.

The effects of the pedestal density, the SOL density and the divertor density on the scalings were presented. They have to be treated carefully due to the high RMSE values in the scalings for ΔW_{MHD} as well as f_{ELM}. Yet, it was shown that the SOL density should not be ignored in future scalings.

It is not obvious from the obtained scalings which parameters ELM losses depend on but trends show that the best scaling parameters for the ELM frequency are T_{ped}, n_{div} and q_{95}. The ELM frequency decreases with any increasing density

parameter. For the electron pedestal density this effect could be due to the fact that a higher n_{ped} value is associated with a longer plasma heating time. f_{ELM} increases with increasing heating power which was expected. There might be more parameters like maybe q_{95} influencing the ELM frequency but no more information can be extracted from the current database. The scalings also indicate that the energy lost due to an ELM can be described using T_{ped}, n_{div}, B_{tor} and Δt_{ELM}. In order to get a better understanding of the phenomena which govern ELM losses, more profiles will have to be fitted and analysed, so that more variations in the dataset's parameters can be evaluated and parameter correlations can be avoided.

Future experiments should collect more data in order to reduce the errors of the scaling parameters' exponents. Those experiments should be performed at a wide range of q_{95} values. A better understanding of the ELM length and the influence of q_{95} on f_{ELM} and ΔW_{MHD} will be helpful to understanding the physics which describe ELM Losses. Parameter scans for those parameters could be performed and more investigations on whether more data leads to a collisionality dependence at ASDEX Upgrade or not would be interesting.

Danksagung

Zahlreiche Personen haben mich bei der Verfassung dieser Arbeit unterstützt. An erster Stelle möchte ich jedoch meinen Betreuern Dank zollen. Sowohl Professor Friedrich Aumayr, welcher sich bereit erklärte, mich als externen Diplomanden in seine Forschungsgruppe aufzunehmen und mich zu betreuen als auch Elisabeth Wolfrum, welche die Betreuung in Garching übernahm, machten die Verfassung dieser Diplomarbeit zu einer äußerst positiven Erfahrung und motivierten mich dadurch dazu, mich für eine Doktorandenstelle zu bewerben. Exzellente Einweisungen in die Materie und nützliches Feedback erhielt ich von Mike Dunne, der außerdem immer einen guten Rat für etwaige Probleme parat zu haben schien.

Meinen anderen Kollegen am IPP möchte ich für einen sehr schönen Aufenthalt am Institut danken. Anregende Diskussionen sowie entspannende und lustige Pausen verdanke ich Jakob Kirschner, Georg Harrer, Sergiu Artene, Matthias Schmidtmayr und Johannes Gnielsen. Dank gilt auch meinen Freunden und Weggefährten, die mich durch das Physikstudium begleitet haben. Namentlich möchte ich an dieser Stelle Daniel Hulme, Vimal Kunnumel, Sebastian Mair, John McCann, Yannick Ulrich, Stefan Wampl und Martin Windisch erwähnen.

Zu guter Letzt möchte ich mich noch bei meiner Familie, meiner wunderbaren Freundin und allen anderen zahlreichen Menschen bedanken, die mich auf meinem Weg begleitet haben.

Bibliography

[1] M G Dunne, S Potzel, F Reimold, M Wischmeier, E Wolfrum, L Frassinetti, M Beurskens, P Bilkova, M Cavedon, R Fischer, B Kurzan, F M Laggner, R M McDermott, G Tardini, E Trier, E Viezzer, M Willensdorfer, The EUROfusion MST1 Team, and The ASDEX-Upgrade Team. The role of the density profile in the asdex-upgrade pedestal structure. *Plasma Physics and Controlled Fusion*, 59(1):014017, 2017.

[2] M.G. Dunne. *Inter-ELM evolution of the edge current density profile on the ASDEX Upgrade tokamak*. PhD thesis, 2013.

[3] R. Dux, V. Bobkov, A. Herrmann, A. Janzer, A. Kallenbach, R. Neu, M. Mayer, H.W. Müller, R. Pugno, T. Pütterich, V. Rohde, and A.C.C. Sips. Plasma-wall interaction and plasma behaviour in the non-boronised all tungsten {ASDEX} upgrade. *Journal of Nuclear Materials*, 390–391:858 – 863, 2009. Proceedings of the 18th International Conference on Plasma-Surface Interactions in Controlled Fusion DeviceProceedings of the 18th International Conference on Plasma-Surface Interactions in Controlled Fusion Device.

[4] R. Fischer et al. 38th EPS Conference on Plasma Physics, Strasbourg, France. P1.072, 2011.

[5] Max-Planck-Institut für Plasmaphysik (IPP). ASDEX Upgrade fusion experiment. https://www.ipp.mpg.de/987491/AUG_engl.pdf. Accessed: 2016-09-15.

[6] Martin Greenwald. Density limits in toroidal plasmas. *Plasma Physics and Controlled Fusion*, 44(8):R27, 2002.

[7] G Janeschitz. Plasma–wall interaction issues in {ITER} . *Journal of Nuclear Materials*, 290–293:1 – 11, 2001. 14th Int. Conf. on Plasma-Surface Interactions in Controlled Fusion Devices.

[8] M. Keilhacker, A. Gibson, C. Gormezano, and P.H. Rebut. The scientific success of jet. *Nuclear Fusion*, 41(12):1925, 2001.

[9] National Physical Laboratory. Cross-sections. http://www.kayelaby.npl.co.uk/atomic_and_nuclear_physics/4_7/4_7_4a.html. Accessed: 2016-08-03.

[10] L.L. Lao, H. St. John, R.D. Stambaugh, A.G. Kellman, and W. Pfeiffer. Reconstruction of current profile parameters and plasma shapes in tokamaks. *Nuclear Fusion*, 25(11):1611, 1985.

[11] A. W. Leonard, A. Herrmann, K. Itami, J. Lingertat, A. Loarte, T. Osborne, W. Suttrop, Divertor Modeling, ITER Database Expert Group, and ITER Divertor Physics Expert Group. ELM Heat Flux in the ITER Divertor. In P. Pavlo, editor, *1998 International Congress on Plasma Physics and 25th EPS Conference on Controlled Fusion and Plasma Physics. Contributed Papers*, volume 22C of *ECA*, pages 670–672, Prague, 1998. European Physical Society.

[12] A. Loarte, M. Becoulet, G. Saibene, R. Sartori, D. J. Campbell, T. Eich, A. Herrmann, M. Laux, W. Suttrop, B. Alper, P. J. Lomas, G. Matthews, S. Jachmich, J. Ongena, P. Innocente, and EFDA-JET Work Programme Collaborators. Characteristics and scaling of energy and particle losses during Type I ELMs in JET H-modes. *Plasma Physics and Controlled Fusion*, 44(9):1815–1844, 2002.

[13] A. Loarte, G. Saibene, R. Sartori, D. Campbell, M. Becoulet, L. Horton, T. Eich, A. Herrmann, G. Matthews, N. Asakura, A. Chankin, A. Leonard, G. Porter, G. Federici, G. Janeschitz, M. Shimada, and M. Sugihara. Characteristics of type I ELM energy and particle losses in existing devices and their extrapolation to ITER. *Plasma Physics and Controlled Fusion*, 45:1549–1569, 2003.

[14] P. J. Mc Carthy. Analytical solutions to the grad–shafranov equation for tokamak equilibrium with dissimilar source functions. *Physics of Plasmas*, 6(9), 1999.

[15] R Neu, K Asmussen, K Krieger, A Thoma, H-S Bosch, S Deschka, R Dux, W Engelhardt, C García-Rosales, O Gruber, A Herrmann, A Kallenbach, M Kaufmann, V Mertens, F Ryter, V Rohde, J Roth, M Sokoll, A Stäbler, W Suttrop, M Weinlich, H Zohm, M Alexander, G Becker, K Behler, K Behringer, R Behrisch, A Bergmann, M Bessenrodt-Weberpals, M Brambilla, H Brinkschulte, K Büchl, A Carlson, R Chodura, D Coster, L Cupido, H J de Blank, S de Peña Hempel, R Drube, H-U Fahrbach, J-H Feist, W Feneberg, S Fiedler, P Franzen, J C Fuchs, G Fußmann, J Gafert, O Gehre, J Gernhardt, G Haas, G Herppich, W Herrmann, S Hirsch, M Hoek, F Hoenen, F Hofmeister, H Hohenöcker, D Jacobi, W Junker, O Kardaun, T Kass, H Kollotzek, W Köppendörfer, B Kurzan, K Lackner, P T Lang, R S Lang, M Laux, L L Lengyel, F Leuterer, M E Manso, M Maraschek, K-F Mast, P McCarthy, D Meisel, R Merkel, H W Müller, M Münich, H Murmann, B Napiontek, G Neu, J Neuhauser, M Niethammer, J-M Noterdaeme, E Pasch, G Pautasso, A G Peeters, G Pereverzev, C S Pitcher, W Poschenrieder, G Raupp, K Reinmüller, R Riedl, H Röhr, H Salzmann, W Sandmann, H-B Schilling, D Schlögl, H Schneider, R Schneider, W Schneider, G Schramm, J Schweinzer, B D Scott, U Seidel, F Serra, E Speth, A Silva, K-H Steuer, J Stober, B Streibl, W Treutterer, M Troppmann, N Tsois, M Ulrich, P Varela, H Verbeek, Ph Verplancke, O Vollmer, H Wedler, U Wenzel, F Wesner, R Wolf, R Wunderlich, D Zasche, T Zehetbauer, and H-P Zehrfeld. The tungsten divertor experiment at asdex upgrade. *Plasma Physics and Controlled Fusion*, 38(12A):A165, 1996.

[16] Y. Nobuta, Y. Hatano, M. Matsuyama, S. Abe, S. Akamaru, Y. Yamauchi, T. Hino, S. Suzuki, and M. Akiba. Tritium retention properties of tungsten, graphite and co-deposited carbon film. *Fusion Engineering and Design*, 89(7–8):1516 – 1519, 2014. Proceedings of the 11th International Symposium on Fusion Nuclear Technology-11 (ISFNT-11) Barcelona, Spain, 15-20 September, 2013.

[17] ITER Physics Expert Group on Confinement, Transport, ITER Physics Expert Group on Confinement Modelling, Database, and ITER Physics Basis Editors. Chapter 2: Plasma confinement and transport. *Nuclear Fusion*, 39(12):2175, 1999.

[18] C.P. Perez, H.R. Koslowski, G.T.A. Huysmans, T.C. Hender, P. Smeulders, B. Alper, E. de la Luna, R.J. Hastie, L. Meneses, M.F.F. Nave, V. Parail, M. Zerbini, and JET-EFDA Contributors. Type-i elm precursor modes in jet. *Nuclear Fusion*, 44(5):609, 2004.

[19] C.C. Petty, J.E. Kinsey, C.T. Holcomb, J.C. DeBoo, E.J. Doyle, J.R. Ferron, A.M. Garofalo, A.W. Hyatt, G.L. Jackson, T.C. Luce, M. Murakami, P.A. Politzer, and H. Reimerdes. High-beta, steady-state hybrid scenario on diii-d. *Nuclear Fusion*, 56(1):016016, 2016.

[20] D. Rittich, C. Hopf, B. Geiger, A. Bock, A. Burckhart, A. Mlynek, C. Rapson, M. Reich, F. Ryter, M. Willensdorfer, Max Planck Society ASDEX Upgrade Team, Max Planck Institute for Plasma Physics, and EUROfusion MST1 Team. Towards a Better Understanding of Neutral Beam Current Drive and Steady State, 2016.

[21] F. Ryter, J. Stober, A. Stäbler, G. Tardini, H.-U. Fahrbach, O. Gruber, A. Herrmann, A. Kallenbach, M. Kaufmann, B. Kurzan, F. Leuterer, M. Maraschek, H. Meister, A.G. Peeters, G. Pereverzev, A.C.C. Sips, W. Suttrop, W. Treutterer, H. Zohm, and ASDEX Upgrade Team. Confinement and transport studies of conventional scenarios in asdex upgrade. *Nuclear Fusion*, 41(5):537, 2001.

[22] R Sartori, G Saibene, L D Horton, M Becoulet, R Budny, D Borba, A Chankin, G D Conway, G Cordey, D McDonald, K Guenther, M G von Hellermann, Yu Igithkanov, A Loarte, P J Lomas, O Pogutse, and J Rapp. Study of type iii elms in jet. *Plasma Physics and Controlled Fusion*, 46(5):723, 2004.

[23] O. Sauter, C. Angioni, and Y. R. Lin-Liu. Neoclassical conductivity and bootstrap current formulas for general axisymmetric equilibria and arbitrary collisionality regime. *Physics of Plasmas*, 6(7), 1999.

[24] P A Schneider, L Barrera Orte, A Burckhart, M G Dunne, C Fuchs, A Gude, B Kurzan, W Suttrop, E Wolfrum, and the ASDEX Upgrade Team. Pedestal and edge localized mode characteristics with different first wall materials and nitrogen seeding in asdex upgrade. *Plasma Physics and Controlled Fusion*, 57(1):014029, 2015.

[25] P.A. Schneider. *Characterization and scaling of the tokamak edge transport barrier*. PhD thesis, 2012.

[26] V.P. Smirnov. Tokamak foundation in ussr/russia 1950–1990. *Nuclear Fusion*, 50(1):014003, 2010.

[27] E. Viezzer, T. Pütterich, G.D. Conway, R. Dux, T. Happel, J.C. Fuchs, R.M. McDermott, F. Ryter, B. Sieglin, W. Suttrop, M. Willensdorfer, E. Wolfrum, and the ASDEX Upgrade Team. High-accuracy characterization of the edge radial electric field at asdex upgrade. *Nuclear Fusion*, 53(5):053005, 2013.

[28] F. Wagner. The physics basis of iter confinement. *AIP Conference Proceedings*, 1095(1):31–53, 2009.

[29] F. Wagner, G. Becker, K. Behringer, D. Campbell, A. Eberhagen, W. Engelhardt, G. Fussmann, O. Gehre, J. Gernhardt, G. v. Gierke, G. Haas, M. Huang, F. Karger, M. Keilhacker, O. Klüber, M. Kornherr, K. Lackner, G. Lisitano, G. G. Lister, H. M. Mayer, D. Meisel, E. R. Müller, H. Murmann, H. Niedermeyer, W. Poschenrieder, H. Rapp, H. Röhr, F. Schneider, G. Siller, E. Speth, A. Stäbler, K. H. Steuer, G. Venus, O. Vollmer, and Z. Yü. Regime of improved confinement and high beta in neutral-beam-heated divertor discharges of the asdex tokamak. *Phys. Rev. Lett.*, 49:1408–1412, Nov 1982.

[30] J. Wesson. *Tokamaks*. Clarendon Press - Oxford, 1997. The Oxford Engineering Science Series.